THE MIKER TECHNIQUE

By

JAMES EDWARD BENNETT

Bachelor of Science
Northwestern State College
Alva, Oklahoma
1957

Master of Science
Oklahoma State University
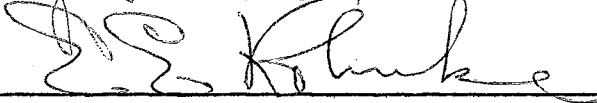Stillwater, Oklahoma
1962

Submitted to the faculty of the Graduate School of
The Oklahoma State University
in partial fulfillment of the requirements
for the degree of
DOCTOR OF PHILOSOPHY
May, 1965

THE MIKER TECHNIQUE

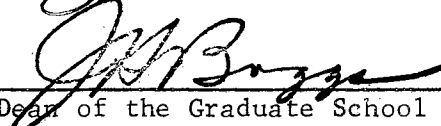Thesis Approved:

Thesis Adviser

Dean of the Graduate School

ii

ACKNOWLEDGEMENTS

TABLE OF CONTENTS

LIST OF TABLES

LIST OF FIGURES

CHAPTER I

INTRODUCTION

Investigations of vaporization processes at high temperatures are complicated by our inability to predict the nature and complexity of vapor species. In recent years, numerous "unexpected" molecular species have been discovered at high temperature and it may be said in general that there is little reason to suspect, even for elemental systems, that the predominant species in the solid (or liquid) will contribute significantly to the vapor composition. The magnitude of this problem is suggested by the various processes which have been observed to accompany vaporization:

Process	Example	Reference
Simple Vaporization	$Au_{(s)} = Au_{(g)}$	(15)
Simple Polymeric Vapor	$4As_{(s)} = As_{4(g)}$	(36)
Mixed Polymeric Vapor	$S_{(s)} = (S_1...S_9)_{(g)}$	(7)
Decomposition	$CdSe_{(s)} = Cd_{(g)} + 1/2\ Se_{2(g)}$	(23)
Disproportionation	$2TiCl_{2(s)} = TiCl_{4(g)} + Ti_{(s)}$	(17)
Complex Vaporization	$3BaO_{(s)} = BaO_{(g)} + Ba_2O_{2(g)}$	(33)
Vapor Phase Reaction	$LiF_{(g)} + RbF_{(g)} = LiRbF_{2(g)}$	(4)

Of these processes, it is not always clear which will be encountered in the determination of the high temperature properties of a given substance, and as one worker[18] has said: "A list of the substances for which the vapor phase molecular species is not known would be almost

1

interminable." It is apparent that vapor pressure and partial pressure measurements, and thermodynamic properties calculable from such measurements, are reliable only to the extent that the complexity of the vapor species is known.

The Knudsen effusion[39, 40, 41] and the Langmuir[42] techniques have been developed most successfully for vapor pressure determinations at high temperatures. In the Knudsen technique the rate of effusion of vapor from a chamber through a small orifice is related to the pressure $\underline{P}$ in the chamber by

$$P = w(2\pi RT/M)^{\frac{1}{2}}/atW, \tag{1}$$

in which $\underline{w}$ is the mass effusing in time $\underline{t}$ through an orifice with cross-sectional area $\underline{a}$, the molecular weight of the effusing vapor is $\underline{M}$, and $\underline{T}$ is the absolute temperature of the vapor in the chamber. The effect of the length of the orifice on the rate of effusion is given by the transmission probability $\underline{W}$[20]. For an ideal orifice, i.e., one with infinitesimal length, $\underline{W}$ is unity; for any real orifice $\underline{W}$ is less than unity.

In the Langmuir technique the vapor pressure is related to the rate of evaporation from an open surface by the equation

$$P = w(2\pi RT/M)^{\frac{1}{2}}/at\alpha \tag{2}$$

which is the same as the Knudsen equation except that instead of the transmission probability, the condensation coefficient $\underline{\alpha}$ appears, and that the area $\underline{a}$ in the Langmuir equation refers to the total evaporating surface.

The Knudsen and Langmuir equations are reliable in the range of molecular flow, i.e., if the mean free path of the molecules is so large that the frequency of intermolecular collisions is negligible.

This criterion defines an experimental range of about 1×10^{-3} to 1×10^{-9} torr for most gases. The lower pressure is not strictly a limit but a pressure below which the measurement of rate of loss of mass is inconvenient. In principle, vapor pressures much lower than 10^{-9} torr could be determined although days or weeks might be required to measure the very low rate of effusion or vaporization.

In both of these techniques the value for the molecular weight $\underline{M}$ must be assumed or must be determined from a separate experiment. For "well-behaved" systems such as pure metals, monomeric vaporization has often been assumed, but the existence of species such as Na_2, Ge_1-Ge_7, and As_4 indicate the danger of this assumption. In special cases thermodynamic arguments may be employed, e.g., the volatilization of Al_2O_3[8], or the system under study may be compared with a chemically similar system of known behavior, e.g., CaF_2[52]. Often, the vapors are condensed on a cooled collector and the sublimate is analyzed. This technique provides only secondary information when vapor polymers, e.g., $(Be)_6$, As_4, S_8, are possibilities.

Much of the work on identification of high temperature species has been done mass spectrometrically. Brewer and Searcy[10], Porter[49], and Inghram and Drowart[34] have reviewed the application of mass spectrometry to high temperature problems, and no effort will be made here to survey this rather large area. However, some aspects will be presented, based largely on the reviews mentioned above. In very general terms, mass spectrometry is concerned with the production of a molecular beam characteristic of the vapor under study, conversion of some of the molecules of the beam into ions which may be identified unambiguously with the neutral species comprising the beam, and finally the resolution

of these ions into their mass components for purpose of quantitative study of each species in the vapor from the sample. If this sequence can be brought about satisfactorily over a suitable temperature range, then it is possible to determine simultaneously:

1. The composition of the gaseous phase,

2. The partial pressure of each of the vapor species, and

3. The variation of each pressure with temperature.

The high sensitivity of a mass spectrometer makes possible the determination of very low concentration vapor species. This knowledge, with appropriate thermodynamic data, allows one to predict the variation of the vapor composition with temperature and pressure. The possibility always exists that an equilibrium vapor contains species which are relatively unimportant at a given temperature, but which increase in concentration, or even become the predominant species, at higher temperatures.* The original work by Chupka and Inghram[13] on the determination of the heats of vaporization of the various species in carbon vapor is now a classic example of this type of application.

In spite of the tremendous versatility and importance of mass spectrometry in studies of high temperature vapors there are difficulties. The production of molecular beams is invariably accomplished by Knudsen effusion or Langmuir evaporation, and uncertainties in these methods obviously are propagated. For example, the high-pressure limit of applicability of the Knudsen and Langmuir techniques has not been demonstrated conclusively. The experimental testing of theories concerning corrections for non-ideal orifices has not been accomplished. Our

---

*For an excellent treatment of such calculations, see Margrave[44].

knowledge of evaporation coefficients[9] and their role in the evaporation process is so meager as to be almost nonexistant. The list could be extended to include the container problem, surface diffusion[63], permeation[16], and others.

The equation

$$P_x = \frac{c}{k} \frac{\sigma(x)}{\sigma(Ag)} \frac{T(x)}{T(Ag)} I_x^+ \tag{3}$$

relates the partial pressure, P_x, of gaseous species x to the ion current, I_x^+, of x^+ observed in the mass spectrometer. The temperature of the effusion cell is $T(x)$, c is a constant dependent on the characteristics of the ion detector and k is a sensitivity calibration of the mass spectrometer in arbitrary units of Ag^{107+} ion current per atmosphere of silver vapor at temperature $T(Ag)$. The quantity $\sigma(x)/\sigma(Ag)$ is the ratio of the relative ionization cross sections of x and Ag. Silver is simply a reference substance convenient for the pressure calibration. In all but the simplest cases the ratio $\sigma(x)/\sigma(Ag)$ must be estimated, a procedure which introduces the largest uncertainty in subsequent data (values of molar heats of sublimation from mass spectrometric data are typically uncertain by 5-10 kcal[49]).

Another problem is that one must decide ultimately which neutral molecule corresponds to a given ion; though some molecules appear to ionize cleanly under electron impact, in general the characteristic fragmentation pattern of an individual molecular species is difficult to establish.

No effort has been made to present a complete description of mass spectrometry, but rather to establish with the reader the fact that, though this tool at present provides the best information about the

complexity of high temperature vapors, it is by no means a "cure-all." Also, it is important to note that any advancement of the Knudsen or Langmuir methods can be expected to improve high temperature mass spectrometry.

It would appear that an invaluable aid for studying high temperature vapors would be direct experimental determination of the molecular weight of the vapor. The problem, however, of measuring the molecular weight of a vapor in the pressure range below 10^{-3} atm., at temperatures generally above $1000^{o}C$, and under vacuum conditions, has proven extremely difficult.

The rather stringent conditions mentioned above, with the increased reactivity among substances at high temperatures, have greatly limited the number of methods which might otherwise be suitable for the determination of the molecular weights of vapors. Nernst[47] and von Wartenberg[61] used a modification of the Victor Meyer[64] method to obtain molecular weights at $1900-2100^{o}$. Their method gave rather good results for water, sodium chloride, mercury, sulfur dioxide and carbon dioxide, but, since it depended on complete and rapid volatilization of the sample, yielded questionable results for tin, and could not be applied in the case of materials with very low vapor pressures at high temperatures.

In 1954, Searcy and Freeman[53] adapted the torsion-effusion method of Volmer[60] to high temperature research. In this method a pair of Knudsen cells are mounted on a very fine torsion wire. The cell orifices are pointed in opposite directions so that effusion produces a torque in the torsion wire and rotates the cell through an angle proportional to the torque. The torsion wire is calibrated and the rotation of the cell may be related to the pressure within the cell by

$$\tau = D\varphi = (q_1 a_1 + q_2 a_2) \, f \, P_T/2 \tag{4}$$

where

τ = torque

D = torsion constant of suspension wire

φ = angle of rotation of cell

q = distance from center of orifice to axis of support

a = cross-sectional area of orifice

f = correction for non-ideal orifice

P_T = pressure within the cell = torsion pressure

No knowledge of the molecular weight of the effusion vapors is required in determination of the torsion pressure. If the rate of effusion is also determined as in a normal Knudsen determination, then the two pressures must be equal, or

$$P_K = P_T = w(2\pi RT/M)^{\frac{1}{2}}/a\,tW \tag{5}$$

in which $\underline{M}$, the molecular weight, is the only unknown quantity.

The apparatus of Searcy and Freeman consisted of a graphite torsion cell enclosed (except for the orifices) in a closely fitting tantalum jacket and suspended on a fine tungsten torsion wire. Radiofrequency induction heating was employed. The vapor pressures of germanium, tin, and silver were determined. Values obtained for the molecular weights of the vapors were 58 ± 16, 91 ± 29, and 260 ± 90, respectively. On the basis of these results, they concluded that germanium and tin vaporize as monomers, but that silver vapor is composed predominantly of higher polymeric forms. The main difficulties reported by Freeman[18] were the nonreproducibility of the torsion constant $\underline{D}$ and the difficulty of locating precisely the null position of the torsion cell. The latter difficulty was the major source of error; it apparently is

inherent with radiofrequency induction heating and results from non-reproducible inductive effects on the torsion cell. In a later effort by Meschi and Searcy[45] to study the volatilization of Al_4C_3 by the torsion-effusion method, but with resistance heating, temperature gradients in the torsion cell introduced new and more serious difficulties.

Sheer[54], who encountered the same difficulties reported by Searcy and Freeman, introduced an innovation of major importance to the torsion technique. Instead of having the closely fitting jacket susceptor attached directly to the torsion cell, he surrounded the cell by a (platinum) chamber, supported independent of the torsion system, and open only to the extent necessary for the effusing vapors to escape, and for the torsion wire to hang freely. Interpretation of the effusion and recoil data is more complicated by this arrangement, because not only the rate of effusion from the torsion cell, but also that from the surrounding chamber, must be accounted for. More important, however, is that this susceptor arrangement provides shielding adequate to eliminate the spurious inductive effects. Sheer studied the $B-B_2O_3$ system by the torsion effusion method, and Hildenbrand[29], with basically the same system, has studied KCl, LiF, LiCl, and BOF.

In 1961, a Langmuir-type recoil momentum device was developed by Bader[1]. The sample material, in the form of a thin foil, is placed on a small tunsten pan suspended from a microbalance. The tungsten pan is heated from below by radiation from a hot tungsten filament. Since the volatility of tungsten is negligible compared to that of the sample, evaporation occurs only from the upper surface. The force exerted by the evaporating molecules results in an apparent mass difference between

the hot and cold sample. This recoil mass, $\underline{m}$, is related to the vapor pressure of the sample by

$$P_R = 2mg/a\alpha, \tag{6}$$

where $\underline{g}$ is the gravitational constant and the other quantities are the same as before. Combination of $\underline{P}_R$ with determination of the rate of evaporation yields the molecular weight $\underline{M}$ in a manner analogous to that of the torsion method,

$$P_K = P_R = w(2\pi RT/M)^{\frac{1}{2}}/a\alpha t. \tag{7}$$

The molecular weight of nickel was determined by this method to be 55.8 ± 30, and nickel (II) oxide was reported as decomposing near $1500^{\circ}K$ with the evolution of monatomic oxygen. The main difficulty was a recoil effect on the pan when empty, which effect Bader attributed to radiation pressure. Difficulty was also reported in the manual operation of the microbalance; this resulted in uncertainties in null position. The technique suffers a serious disadvantage in that temperature measure-ments with an optical pyrometer must be corrected for the emissivity of the sample. The torsion method does not suffer this disadvantage because the orifice of the torsion cell or an auxiliary hole serves as an excellent blackbody for pyrometric measurements.

It is apparent that both of the methods just discussed have great utility for high temperature vaporization studies. However, from the rather large errors associated with the molecular weights, and from the comments of the authors regarding experimental difficulties, it is equally apparent that more research is needed on recoil techniques.

The present research has been concerned with the development of a new recoil technique for the simultaneous determination of vapor pressures and the average molecular weight of the species which comprise

the vapor at high temperatures.

As further statement of the problem, and to preface Chapter II, which includes the theoretical aspects of the new tecnhique mentioned above, it should be pointed out that a thorough description of the technique will require considerable material for which the author can claim no originality. The author is fortunate in this respect, however, because his work has been carried out more or less concurrently, and in the same laboratory, as the theoretical work of Freeman and Edwards[20], much of which applies directly to the techniques to be described.

CHAPTER II

THE MIKER TECHNIQUE

For brevity a special name has been coined. It is formed from the first letters of several key words which describe the technique: The Microbalance-Inverted Knudsen Effusion-Recoil technique — the MIKER technique.

The principal innovation of the Miker technique is the inverted effusion cell shown in Figure 1. The cell is suspended from a microbalance into a suitable furnace and effusion occurs only in the downward ($-Z$) direction away from the microbalance. The conservation of momentum requires that the cell receive, in the $+Z$ direction (upward), momentum identical in magnitude to the momentum possessed by the effusing molecules in the $-Z$ direction. The rate of change with time of this momentum is defined as the recoil force. At a constant temperature the recoil force is constant and the variation of the weight of the cell with time will yield the rate of effusion. After the rate of effusion has been established at a particular temperature, the power to the furnace is suddenly reduced to zero, and the cell allowed to cool rapidly so as to minimize further effusion. The cell immediately appears "heavier" to the microbalance due to the rapid disappearance of the recoil force. Combination of this apparent gain in mass by the cell with the rate of effusion data can yield information regarding vapor and decomposition pressures, as well as the average molecular

11

MICROBALANCE

VACUUM
ENVELOPE

FURNACE
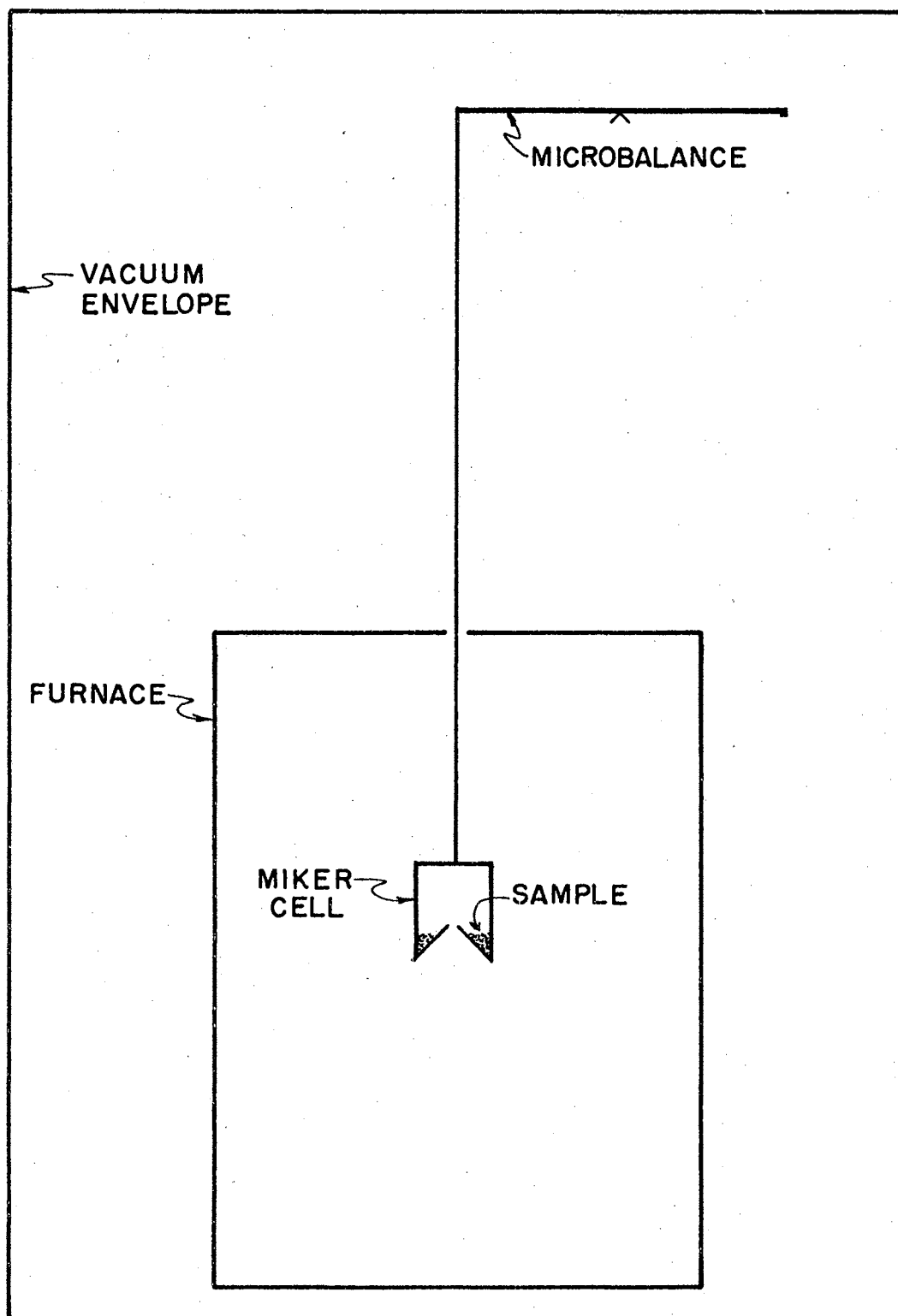
MIKER
CELL   SAMPLE

Figure 1. Schematic Representation of Apparatus for Miker Technique.

weight of the vapor; the pertinent relations among the quantities will now be considered.

The Recoil Force and the Recoil Pressure. The cosine law of molecular flow[20] may be stated: the number dN_ω of molecules which cross an incremental plane surface ds per second and flow into an incremental solid angle $d\omega$ which lies at the angle θ from the normal to the surface is given by

$$dN_\omega = \sigma \, \upsilon \, ds \, \cos\theta \, d\omega \qquad (8)$$

in which υ is the incident density, i.e., the number of molecules which impinge each second on a unit surface in the gas, and σ is a proportionality constant.[†] If the normal to the surface is chosen as the Z axis for conventional transformation of $d\omega$ into spherical co-ordinates[38], one has

$$d\omega = \sin \, \theta \, d\theta \, d\varphi. \qquad (9)$$

Since none of the effects to be considered depend on the angle φ, this equation is immediately integrated over φ from 0 to 2π with the result

$$d\omega = 2\pi \, \sin \, \theta d\theta. \qquad (10)$$

The effusion of molecules through an orifice, depicted in Figure 2, also constitutes a transfer of momentum across the plane of the orifice. The rate of momentum transfer for those molecules which have speed c and which effuse through elemental area ds into $d\omega$ at angle θ from the orifice axis is $mc \, dN^*_\omega$; dN^*_ω corresponds to dN_ω of equation (8) except for the star superscript that here and subsequently will refer to those molecules having speed c. We shall be particularly interested in the momentum component which is parallel to the axis of the orifice because

---

[†]This derivation follows closely that of Freeman and Edwards, in which they show that $\sigma = 1/\pi$.
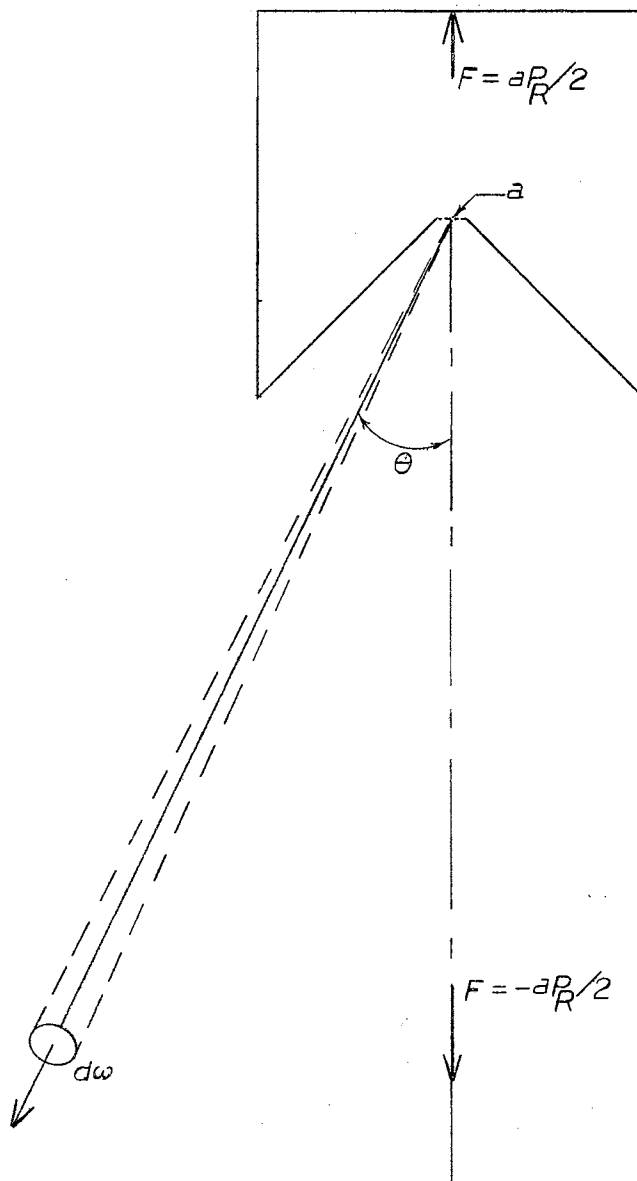
Figure 2. Momentum Transfer by Molecular Flow
from a Conical Orifice.

this is the only component which is detectable with the microbalance. Also, because of the symmetry of the Miker cell, the resultant of all non-vertical components is zero. The rate of transfer for the vertical component is

$$mc \cos \theta \ dN_{\omega}^{*}. \tag{11}$$

The net transfer of momentum across a plane indicates the presence of a force and, of course, an equal and opposite reaction force. Microscopically, the force is just that which would be produced by impingement and condensation on a surface of the effusing molecules, and the reaction force is that which is exerted by molecules, equal in number to those which effuse but with velocity vectors opposite in direction, impinging on the cell wall opposite the orifice. The force component dF_{ω}^{*}, parallel to the orifice axis, of both the force in the effusing beam and the reaction, or recoil, force is equal to the net rate of transfer of the momentum component parallel to the axis; hence, from equation (11) we have

$$dF_{\omega}^{*} = mc \cos \theta \ dN_{\omega}^{*} \tag{12}$$

Integration of $\underline{ds}$ over the orifice area $\underline{a}$, and conversion to spherical coordinates give

$$dF_{\omega}^{*} = 2mca\upsilon^{*} \sin \theta \cos^{2} \theta d\theta. \tag{13}$$

Subsequent integration over $\underline{\theta}$ from $\underline{0}$ to $\underline{\theta}$ and substitution of $\underline{\upsilon}^{*} = \underline{n}^{*}\underline{c}/4$ (Kennard[38]), where $\underline{n}$ is the number density of the gas, give

$$F_{\theta}^{*} = an^{*} mc^{2}(1 - \cos^{3} \theta)/6; \tag{14}$$

$F_{\underline{\theta}}^{*}$, of course, is the recoil force (or beam force) which is parallel to the orifice axis and which results from those molecules with speed $\underline{c}$ which effuse into the cone defined by $\underline{\theta}$. The total force $\underline{F}_{\theta}$ exerted by all effusing molecules is just the summation of equation (14) over all

speeds,

$$F_\theta = \sum_{c=0}^{\infty} F_\theta^* = a(1 - \cos^3 \theta)(mn/6) \sum_{c=0}^{\infty} (n^*/n)c^2 \tag{15}$$

$$= a(1 - \cos^3 \theta)n m \overline{c^2}/6. \tag{16}$$

If we now employ further results from kinetic theory[38],

$$P = n m \overline{c^2}/3,$$

and

$$\overline{c^2} = \overline{c}^2(3\pi/8),$$

we have

$$F_\theta = a(1 - \cos^3 \theta)P/2 = \pi N m \overline{c}(1 - \cos^3 \theta)/4, \tag{17}$$

where $N = \nu a$; or if $\underline{P}_R$ designates the pressure determined by measuring the recoil force,

$$P_R = 2F_\theta/a(1 - \cos^3 \theta). \tag{18}$$

The _total_ recoil force $\underline{F}$ and the corresponding expression for $\underline{P}_R$ are given by equations (17) and (18) with $\theta = \pi/2$.

$$F = aP_R/2 = \pi N m \overline{c}/4,$$

$$P_R = 2F/a. \tag{19}$$

Correction Factors $\underline{f}$ and $\underline{W}$. A recoil-force correction is required because of the diminution of flow and of the partial collimation of velocity vectors of effusing molecules, by orifices of finite length. Both of these effects are corrected for by the recoil-force correction factor $\underline{f}$, which has been derived for conical orifices by Freeman and Edwards[20]. Table I lists some of their values of $\underline{f}$ for conical orifices of various $\underline{L/r}$ (length/small end radius) and $\underline{T}$ (off-axis angle; Figure 11). Also included are the corresponding values for the transmission probability $\underline{W}$, which measures the probability that a molecule, having entered the conical orifice, will effuse from it.

The force factor $\underline{f}$ may be explicity incorporated into a modification of equation (19):

$$P_R = 2F/af. \tag{20}$$

TABLE I

TRANSMISSION PROBABILITIES, $\underline{W}$,
FOR CONICAL ORIFICES[b]

$(L/r)^a$	T^a, deg.						
	0°	10°	20°	30°	40°	50°	60°
.1	0.9524	0.9673	0.9786	0.9869	0.9927	0.9964	0.9986
.2	0.9092	0.9384	0.9603	0.9761	0.9870	0.9939	0.9977
.4	0.8341	0.8894	0.9306	0.9597	0.9790	0.9904	0.9968
.6	0.7712	0.8499	0.9079	0.9481	0.9739	0.9888	0.9963
.8	0.7178	0.8176	0.8903	0.9396	0.9704	0.9878	0.9962
1.0	0.6720	0.7908	0.8764	0.9334	0.9681	0.9870	0.9959
2.0	0.5142	0.7058	0.8370	0.9177	0.9629	0.9857	0.9957
4.0	0.3566	0.6348	0.8108	0.9095	0.9608	0.9853	0.9957
6.0	0.2754	0.6051	0.8022	0.9073	0.9603	0.9852	0.9957
8.0	0.2253	0.5895	0.7984	0.9065	0.9601	0.9851	0.9956
10.0	0.1909	0.5802	0.7963	0.9060	0.9599	0.0851	0.9956

RECOIL FORCE FACTORS $\underline{f}$ FOR DIVERGING
CONICAL ORIFICES[b]

$(L/r)^a$	T, deg.						
	0°	10°	20°	30°	40°	50°	60°
.1	0.9683	0.9861	0.9995	1.0090	1.0146	1.0167	1.0157
.2	0.9373	0.9720	0.9982	1.0163	1.0269	1.0307	1.0283
.4	0.8785	0.9445	0.9941	1.027	1.0468	1.0527	1.0473
.6	0.8247	0.9190	0.9894	1.0365	1.0622	1.0692	1.0609
.8	0.7762	0.8960	0.9849	1.0434	1.0744	1.0821	1.0712
1.0	0.7327	0.8756	0.9809	1.0492	1.0845	1.0923	1.0790
2.0	0.5725	0.8035	0.9682	1.0687	1.1163	1.1236	1.1021
4.0	0.4024	0.7381	0.9633	1.0908	1.1462	1.1504	1.1205
6.0	0.3125	0.7107	0.9660	1.1044	1.1618	1.1636	1.1289
8.0	0.2564	0.6970	0.9699	1.1140	1.1720	1.1717	1.1338
10.0	0.2177	0.6892	0.9736	1.1212	1.1793	1.1774	1.1371

[a] See Figure 11.

[b] From Freeman and Edwards[20].

Determination of M^*. The recoil mass m is defined as the mass which, under the acceleration of gravity g, counterbalances the recoil force acting on the cell. Therefore, the recoil force F can be related to the recoil mass m by $F = mg$, which, with equation (20) yields

$$P_R = 2mg/af. \qquad (21)$$

Measurement of the recoil mass therefore determines the pressure P_R of the vapor effusing from the Miker cell. Furthermore, this determination requires no knowledge of the molecular weight M of the effusing vapor.

We may also relate the vapor pressure to the rate of effusion data by equation[†] (1)

$$P_K = \omega(2\pi RT/M)^{\frac{1}{2}}/atW; \qquad (1)$$

but we have also $P_R = P_K$, and therefore

$$P_K = P_R = \omega(2\pi RT/M)^{\frac{1}{2}}/atW,$$

or $\qquad 2mg/af = \omega(2\pi RT/M)^{\frac{1}{2}}/atW. \qquad (22)$

Equation (22) combines the recoil force and rate of effusion data and represents the basic equation of the Miker technique; it can be solved directly for the average molecular weight M of the vapor species.

Freeman[18] has shown that an equivalent and more informative treatment is to assume a value M_K for M in equation (1), and calculate P_K. Then P_K and P_R are related in the following way to yield the actual (average) molecular weight M^*:

$$M_K = P_K^2 t^2 a^2 / 2\pi\omega^2 RT; \qquad (1)$$

[†]At a given temperature, a given substance has a unique vapor pressure, of course, and under these conditions $P_K = P_R$. However, here and subsequently, the pressures associated with recoil data will be denoted by P_R and those associated with rate of effusion data (the Knudsen equation) will be denoted by P_K.

$$M^* = P_R^2 t^2 a^2 / 2\pi\omega^2 RT. \tag{23}$$

Combination of (1) and (23) yields

$$M^* = M_K (P_K/P_R)^2. \tag{24}$$

The value for $\underline{M}^*$ from equation (24) gives information directly from the complexity of the vapor. If $P_R = P_K$, then $M^* = M_K$, and the molecular weight of the vapor species is that assumed in the Knudsen equation; if $M^* = 2M_K$, then the molecular weight of the vapor species is just twice that which was assumed for the Knudsen equation, etc. If $\underline{M}$ and $\underline{M}^*$ are related in a non-integral manner, the vapor species is more complex than that of just monomers, or just dimers, etc., and the stoichiometry of the possible vaporization products must be considered. Now $\underline{M}^*$ becomes a kind of average molecular weight which is related to the molecular weights of the effusing species by

$$M^* = (\omega_1 M_1^{-\frac{1}{2}} + \omega_2 M_2^{-\frac{1}{2}} + \cdots \omega_n M_n^{-\frac{1}{2}})^{-2} \tag{25}$$

in which $\underline{\omega}_n$ and $\underline{M}_n$, for example, are the weight fraction and molecular weight of the $\underline{n}^{th}$ species.

It is important to emphasize that failure to employ both $\underline{W}$ and $\underline{f}$ could introduce a serious error in the molecular weight calculation. For example failure to make the force correction for a cell with $T = 30^\circ$ and $L/r = 4$ would result in an error of about 20% in the molecular weight.[†]

Effusion During the Cooling Period. Ideally, once the rate of effusion has been established at a particular temperature, power to

---

[†]Because such magnitudes are involved, experimental testing of W and f is of much interest to work of the present kind. Other workers in this laboratory are currently engaged in investigation designed to determine the validity of derivations which yield W and f.

the furnace is cut off, effusion ceases, and the recoil force is then measured. For any real system, however, cooling will not be instantaneous and some effusion will occur during the cooling period. This effusion, if left unaccounted, would introduce an error in the measurement of the recoil force as is illustrated in Figure 3. The effusion that occurs after cutting off the power constitutes a weight loss, while the disappearance of the recoil force is an apparent weight gain. It is the algebraic sum of these two effects which is actually measured by the microbalance.

It is impossible to separate experimentally the actual recoil curve into its components, the effusion curve and the pure recoil curve (Figure 3). An expression is derived in Appendix A, however, which relates the rate of effusion to the rate of cooling of the Miker cell, thereby allowing calculation of the mass m_c which effuses during the cooling period.

The recoil pressure P_R may be written in terms of m_c. From equation (21) we have

$$P_R = 2gm_i/af; \tag{26}$$

the subscript on m_i refers specifically to the recoil mass which would be observed with instantaneous cooling. But, from Figure 3 and the previous discussion, we have

$$m_i = m + m_c; \tag{27}$$

therefore,

$$P_R = 2g(m + m_c)/af. \tag{28}$$

To summarize, the quantities which must be measured are the temperature, the rate of effusion, and the recoil force. Other quantities which must be known are the mass m_c which effuses during the cooling
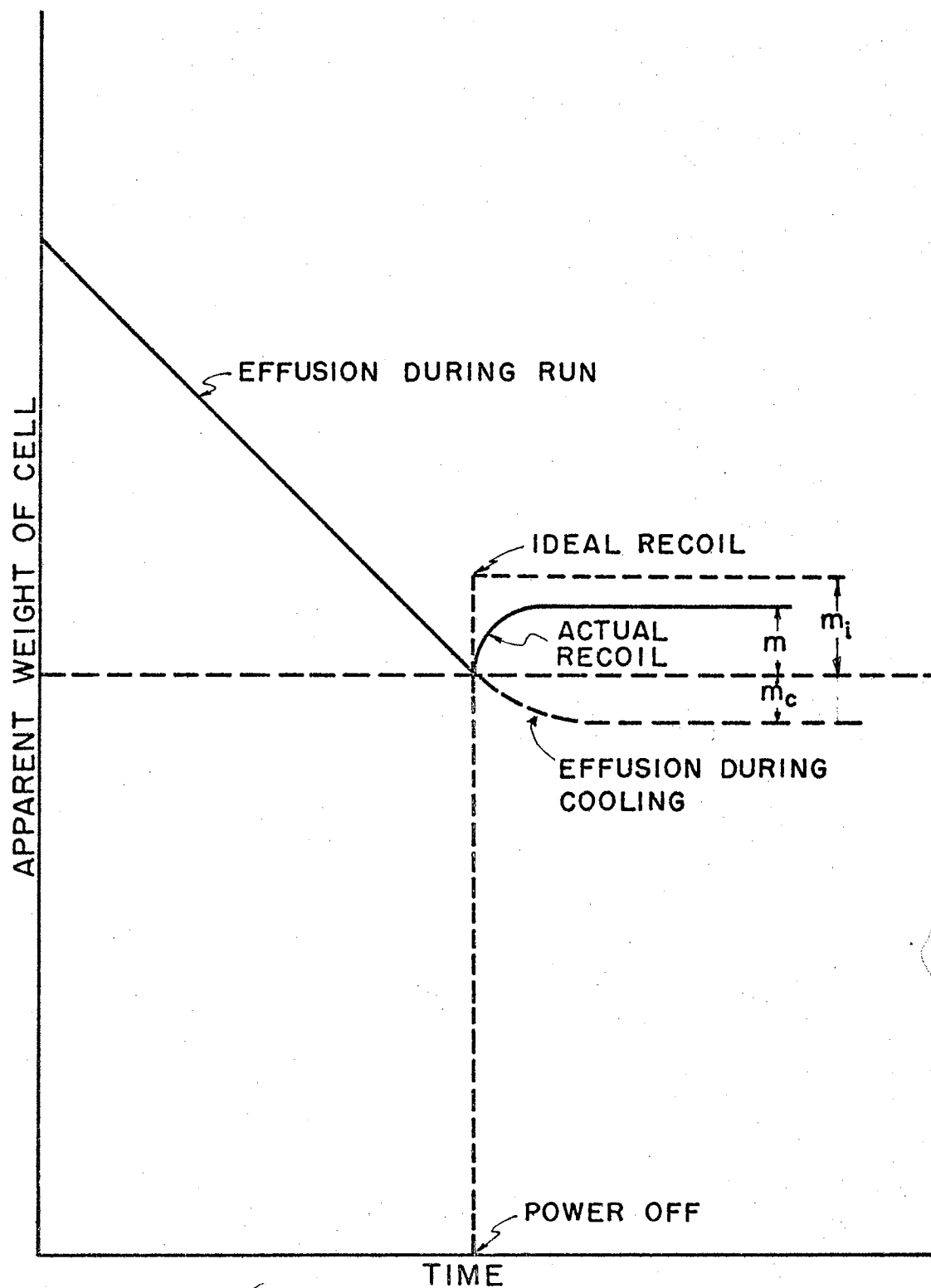
Figure 3. The Effect on the Recoil Mass of Effusion which Occurs During the Cooling Period.

period, the cell parameters, and the correction factors, $\underline{W}$ and $\underline{f}$.

CHAPTER III

DESIGN AND CONSTRUCTION OF THE APPARATUS

The Microbalance. Effusion from a cell in which the pressure is 10^{-3} to 10^{-6} atm produces forces in the range 1 to 10^{-3} dynes, or 10^{+3} to 1 microgram weight. To measure these forces with a precision of one per cent a balance is needed with a sensitivity of at least 10^{-6} g, and preferably 10^{-7} g. A rather small Miker cell will have a mass of 2-5 g. Therefore a balance suitable for the Miker technique must have the characteristics: (1) operable in vacuum; (2) sensitivity of about 10^{-6} g; (3) load capacity of at least 5 g. No restrictions need be imposed because of high temperatures; with suitable shielding the balance can be operated as a "room temperature" instrument.

To the conditions above must be added the desire that the balance should be adaptable to automatic control and therefore should operate as a null instrument. The advantages of an automatically recording instrument are more than just convenience of operation. A continuous trace on a recorder sheet provides a phenomenological account of the effusion and recoil processes. Greater precision would also be expected from an automated instrument.

A pivotal-type microbalance constructed for this research is depicted in Figure 4; it bears the laboratory designation VMB-1. Several new features have been introduced. The balance beam $\underline{A}$ is a 6.3-in. length of stainless steel tubing with 0.094-in. i.d. and 0.120-in. o.d.

23

Figure 4. The Vacuum Microbalance, VMB-1.

Two polished diamond points C with tip radius 0.0007 to 0.001 in. serve as center pivots. The diamond points, (mounted on small jewel screws, C.), were obtained from the Moser Jewel Company. Holes were drilled and tapped in an aluminum mounting block B to accomodate the jewel screws so that the pivot tips are 0.5000±0.0005 in. apart. The mounting block is attached to the beam with epoxy adhesive. Polished-sapphire cups, S, from the same source and also mounted on jewel screws, serve as bearing surfaces for the diamond pivots. The cups, or vees, are mounted in a block so that their minima are separated by 0.5000±0.0005 in. in the horizontal plane. Point and vee alignment is fixed by lock screws D and U, respectively.

Supports typically used at the ends of the beam are the hook type[11], the quartz-on-tungsten-wire type[32], or the two-pivot type[50]. To minimize friction and to simplify the problem of adjusting all bearing surfaces to be in a common plane, VMB-1 has a single pivot H mounted, tip upward, at each end of the beam; these pivot tips and the center ones are adjusted so that they are in a common plane within 0.0005 in. With only one pivot at each end of the beam, this adjustment is relatively simple. The surface which bears on the end diamond pivots is again a sapphire cup, L (inset, Figure 4 - only one is shown). A stirrup P is attached by thin aluminum strips M to the sapphire cup at two points in a horizontal plane slightly below the point of contact between the tip of the pivot and inverted sapphire cup. Loads are suspended from the cross-piece of the stirrups. The aluminum mounting blocks for the diamond end-pivots are sealed in the ends of the hollow beam with epoxy adhesive. An opening is provided at each end for evacuation of the hollow beam.

A thin front-surface mirror $\underline{E}$, with 0.25-in. diameter is mounted on top of the center aluminum block and midway between the center pivots. About 0.5-in. from one end of the beam, a small aluminum block $\underline{K}$ is attached by epoxy adhesive to the bottom of the beam. This serves as a mount for 0.062-in. diameter Cunife wire magnets $\underline{J}$. The magnets are held in the mounting block by a tight frictional fit which permits interchange of magnets with various lengths. When properly installed, a given magnet is perpendicular to the beam and protrudes equal distances on each side of the beam.

The base (Figure 5) for the balance was constructed from 0.25-in. thick brass. The sapphire cups $\underline{F}$ for the center pivots are mounted on adjustable screws which are accommodated by a brass block attached to the base plate. The base plate has in the bottom, three V-grooves which rest on ball bearings $\underline{D}$ mounted in fixed sockets of a second brass plate. This is to assure that the balance and base plate can be removed and later returned precisely to the original position. Two screw-adjustable knife-edge beam rests, $\underline{R}$, Figure 4, are located in the base plate. The second plate rests on four sharply pointed screws $\underline{B}$ which serve as a leveling device.

Discussion -- VMB-1 Sensitivity. Theoretical analysis[24, 62] of the simple beam-type balance (Figure 6) gives as the equation for the sensitivity, $d\theta/dz$:

$$d\theta/dz = \mathcal{l}/[\mathcal{G}S + 2aP]$$
(29)

where

θ = turning angle in radians,

P = load in grams on right side,

P + z = load in grams on left side,
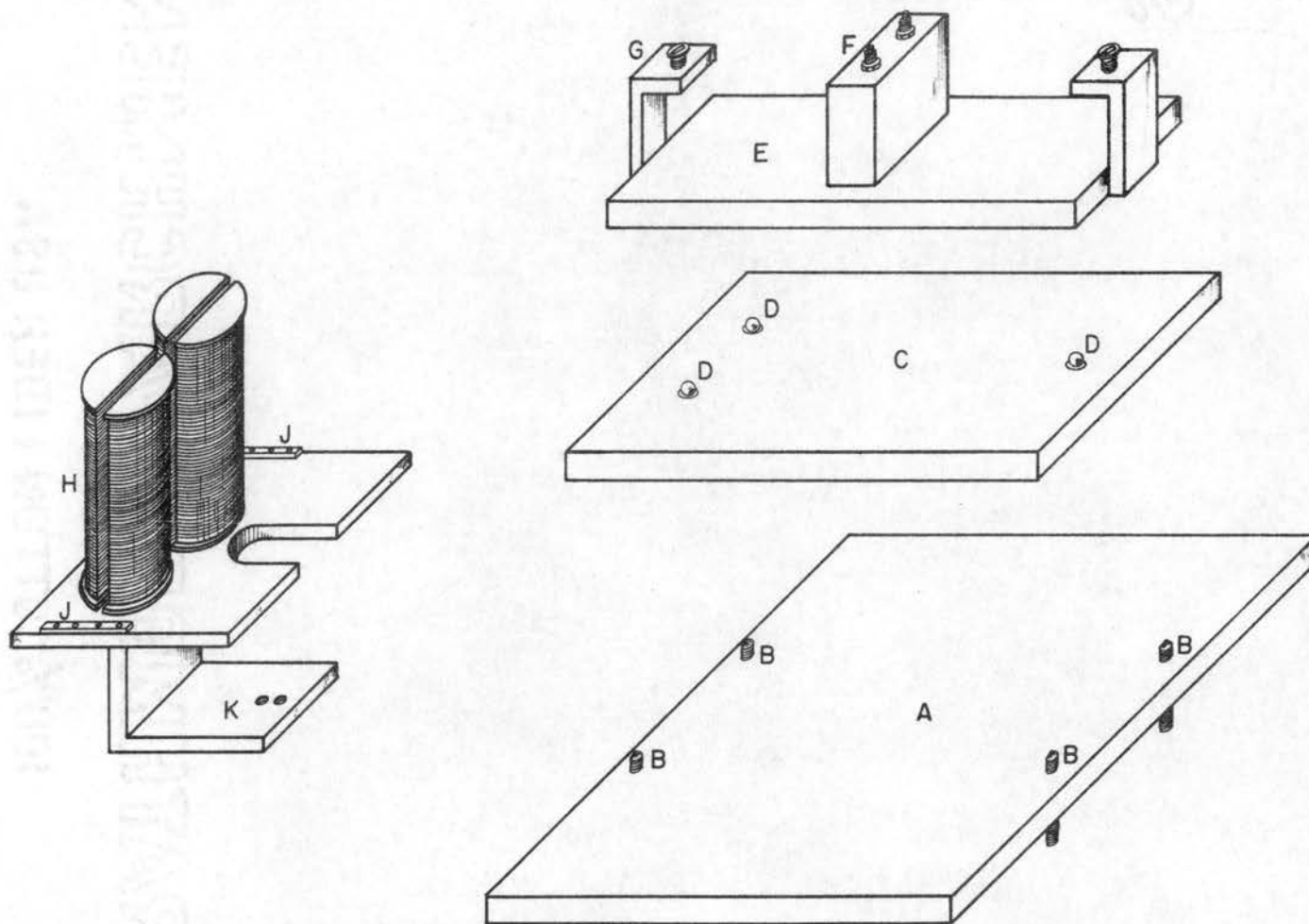
Figure 5. The Base Assembly for Supporting, Leveling, and Providing Kinematic Alignment of the Microbalance.

2ℓ = length of beam in cm;

G = weight of beam in grams,

S = vertical distance from center of gravity of beam to plane of support (cm),

a = vertical distance from center line of beam, to plane of support (cm).

To simplify the discussion, the term a will be considered first. When the bearing points are coplanar with the center line of the beam, a = 0, and the quantity $a(2P)$ becomes 0. This is the first step toward making the balance sensitivity independent of load. The next is to make certain that S is not a function of the load. Ideally, the points of contact at the center pivots and those at the end pivots should be in a common horizontal plane which bisects the beam. If the beam bends under load, the situation is more complex. For any system to be mechanically stable, the center of mass must be below the center of support. Thus if the vertical distance separating the center of mass and the center plane of support decreases with increasing load, the balance actually becomes more sensitive. If this same distance increases with increasing load, the balance becomes less sensitive.

As mentioned, the four point contacts were adjusted to within 0.0005 in. of the plane which bisects the beam; therefore, a = 0 ± 0.0005 in. Previously, the beam was tested for bending under load by fastening it securely at the mid-point and suspending rather large masses from one end. With a mass of 50 g suspended from one end, no deflection within ± 0.0005 in. was observed. This result, with the fact that in normal use the maximum load suspended from each end will be 5 g , indicates the balance sensitivity to be independent of beam-bending effects.

It follows that equation (29) may be simplified to

$$d\theta/dz = \mathcal{L}/GS,\qquad\qquad(30)$$

and the theoretical sensitivity may be calculated from a knowledge of
$\mathcal{L}$, G, and S. Rather than calculate S, the expression for the period
of oscillation of the beam[62], which contains S, will be employed. The
period, T seconds, of the beam oscillating about its center pivots is
given by

$$T = 2\pi I_B/gGS,\qquad\qquad(31)$$

where I_B is the moment of inertia, g is the gravitational constant,
and G and S have been defined. Equation (31) is valid only under condi-
tions of no load and describes the __natural__ period of the balance.

The period T was measured to be 4 sec; I_B calculated is 90 g cm^2;
G is 4.3 g. The value for S may now be calculated from equation (31)
to yield $S = 0.03$ cm, which is consistent with S values of other micro-
balance designs (Walker[62], $S \cong 0.01$ cm; Gulbransen[24], $S \cong 0.04$ cm).

The sensitivity may now be calculated from equation (30), to yield
$d\theta/dz = 6.6 \times 10^{-5}$ radians/μg. This means that for $\mathcal{L} = 8.5$ cm, a 1 μg
load should result in beam deflection of approximately $8.5 \times 6.6 \times 10^{-5}$ cm
or about 6.0 μ. Methods for detecting beam deflections of the order of
1 μ or less will be discussed in a later section, but assuming this
ability for the moment, the balance sensitivity appears to be well within
the desired limits which were quoted at the beginning of this chapter.

The best set of dimensions for a given microbalance is difficult
to assess. An attempt was made to optimize the various balance para-
meters by the method of Lagrangian multipliers[43], with the restrictions
that the sensitivity and the beam length be maxima, while the beam
weight and the distance from the center of gravity to the center

POINT OF SUPPORT

TERMINAL SUPPORT

TERMINAL SUPPORT

B

D

a

s

l

φ

A

l

C

S

S

P

MIDPOINT OF AB

CENTER OF GRAVITY
OF BEAM

P + z

LOAD ON LEFT SIDE

LOAD ON RIGHT SIDE
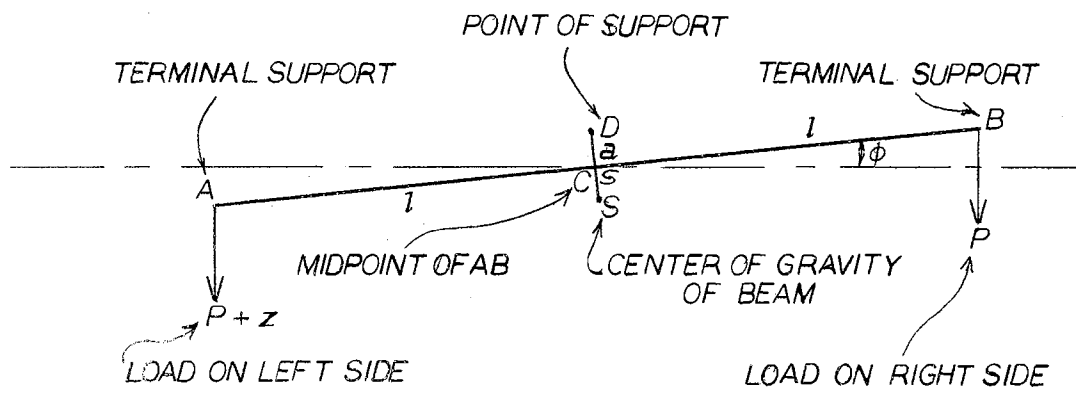
Figure 6. Diagram of a Simple Beam Balance.

of support be minima. But this analysis fast became too formidable, because of the large number of variables involved. The problem is perhaps compatible to computer solution, but was not pursued in this work. Walker[62] designed a microbalance by choosing an initial desired sensitivity and then adjusting the remaining parameters mathematically. The actual sensitivity realized was 65% less than that desired, but even this closeness is remarkable.

Choice of Materials. Stainless steel tubing was chosen as the beam material for VMB-1 because of its lightness, strength, resistance to corrosion, and the precision which is attainable in machining it and attaching components to it. Quartz is undoubtedly superior as a beam material in many respects, e.g., chemical inertness, coefficient of thermal expansion, lightness, etc., but quartz was eliminated as a beam material because of the difficulty of working it with precision. It might be mentioned, however, that precision quartz tubing, recently commercially available, was seriously considered. The components attached to the beam could still be of aluminum, thus retaining the advantage of relatively easy constructional precision.

Invar tubing was also considered as a beam material. Gulbransen and Andrew[25] employed this material to construct a simple (solid) beam balance for the study of fast chemical reactions. Because of its low temperature coefficient of expansion, Invar is well suited as a beam material when the balance is to be subjected to temperature changes. The VMB-1 operates at a relatively constant temperature, however, and Invar offers no special advantage. Furthermore, its relatively high density and the fact that it is highly ferromagnetic further eliminate Invar as a choice for VMB-1.

Contrary to manufacturer's claims, the stainless steel tubing was slightly ferromagnetic. As a result, some "sticking" of the beam on the steel knife-edge arrests was experienced. Changing to brass arrests eliminated this problem.

There are several reasons for the selection of diamond pivots and sapphire vees. The most important factors which determine the feasibility of any pivot-vee combination are friction, pivot load, and vibrations. Theoretically, friction is minimized by minimizing the contact area between the pivot and the vee. This principle suggests the use of infinitely sharp points, but in practice pivot points must be rounded because exceptionally sharp points deform under load. This factor more than any other limits the ultimate ratio of load capacity to sensitivity in microbalance design. Optimum design requires use of that material which yields the largest number for the ratio: load at which pivot destortion occurs/pivot radius. Diamond appears a clear choice, and Stott[58] has determined empirically that the minimum pivot radius suitable for a 5 g load is about 0.003 cm.

Once the pivot dimensions are selected, it is a rather simple matter to select the vee. The vee radius should be 2 to 3 times the pivot radius to balance the necessity for minimum contact area with the need to avoid excessive lateral play between the pivot and vee.

The depth and angle of the vee are important when vibrations are likely to exist. Deep vees with relatively steep angles are considered superior to shallow or wide-angle vees when vibrations must be accomodated.

The hardness, ready availability, and easy adaptibility of sapphire vees make them an excellent choice for the diamond pivots. Another

reason for choosing the diamond-sapphire combination is that, in spite of their apparent advantages, no previous workers have stressed these materials as microbalance components, though Honig[32] suggested the possible use of diamond pivots, and Cochran[14] used a sapphire cone-tungsten point combination.

Magnetic Balancing System. The method for achieving magnetic coupling for control of the balance beam position is a modification of methods employed by Simon, Shierrer, and Ritter[55], and by Gerritsen and Damon[21]. Each end of the Cunife magnet extends halfway into the gap between a pair of hemicylindrical coils (Figure 5). Each coil has approximately 2000 turns of A.W.G. No. 30 copper wire on a solid copper core. The gap between the flat sides of a pair of coils is 0.25 in. Control of the position of the balance beam is achieved by varying the current through the four coils which are wired in series. A polarity reversing switch makes it possible to drive the end of the beam to which the magnet is attached in either the downward or upward direction.

To minimize problems arising from poor heat dissipation in vacuum, the coils are mounted on a copper block which serves as a heat sink. Difficulty from overheating (and from consequent variation of the coil resistance) was experienced in earlier models in which about 3500 turns per coil of A.W.G. No. 36 copper wire were wound on four Lucite cores.

The magnet is mounted on the same end of the beam from which the Miker cell is suspended. This results in a constant-load balance; as the mass of the Miker cell and sample decreases, a compensating increment of current is provided to the coils to retain the null. Consequently, the balance always supports the same net load; if the magnet were mounted on the opposite end of the beam, this would not be the case.

Discussion - Automatic Control. The problem is stated simply:

The (null) position of the balance beam must be controlled under condi-

tions of changing load and without human intervention. The process for

achieving control will be described first in general terms and then

identified with the control system components.

In order to discern when the control system has done its work, some

measurement must be performed. If the desired position of the beam is

indicated by the value θ_i of some measurable quantity, then θ_i is called

the (desired) input. The quantity θ might correspond to actual beam

deflection for example, or as will be shown, to the voltage output of

a Wheatstone bridge circuit. The actual instantaneous value of θ is

termed the output, θ_o. The instantaneous difference $(\theta_i - \theta_o)$, between

the input (desired value) and the output (achieved value) is called

the instantaneous error. With these terms, the control process is the

following:

1. The quantities θ_i and θ_o are measured and the error $(\theta_i - \theta_o)$

is obtained[*];

2. The error $(\theta_i - \theta_o)$ is fed into the control system in a suitable

physical form, to initiate control action that tends to reduce the

error to zero.

3. Control action maintains $\theta_i = \theta_o$.

The technique of comparing the desired value with the actual value

at any instant is known as "feedback," and control action achieved in

this manner is called "closed loop" or "feedback" control.

---

[*] Almost all control systems incorporate devises which measure
$(\theta_i - \theta_o)$ directly[48].

Control System I. Two variations were tried in efforts to achieve automatic control. The first is depicted in Figure 7. A light beam from a tungsten-filament lamp passes through a slit formed by two razor-blades and is reflected onto the mirror of the balance beam from which it is reflected onto a photoconductive null sensor. The null sensor, designed as suggested by Shuttleworth[55], consists of two truncated prisms of single-crystal cadmium sulfide placed base to base and separated by a thin Mylar sheet. Ohmic contacts to the crystals were made with indium to which copper leads are attached with conductive (silver-filled) epoxy adhesive. The crystals constitute two legs of a Wheatstone bridge circuit, the output of which is an approximately linear function of the location of the spot of light on the vertical axes of the crystals. Thus the input to the amplifier is approximately proportional to the position of the balance beam, i.e., the correction signal is proportional to the error. A servomotor driven by the output of the amplifier operates a ten-turn potentiometer which regulates the grid voltage of a pentode operated as a cathode follower. The four coils are in the cathode circuit of the pentode. Interaction between the magnetic field of the coils and the "Cunife" magnet on the balance beam completes the servo loop.

Control System II. (Figure 9). Several components are retained from System I: the Cunife magnet; the coils; the tungsten-filament lamp; the razor-blade slit and mirrors; and, of course, the balance beam. The other components which appear in System II are commercially available. A short description of each major component and its expected advantages follows.

The Photopot is in essence a light actuated potentiometer, but
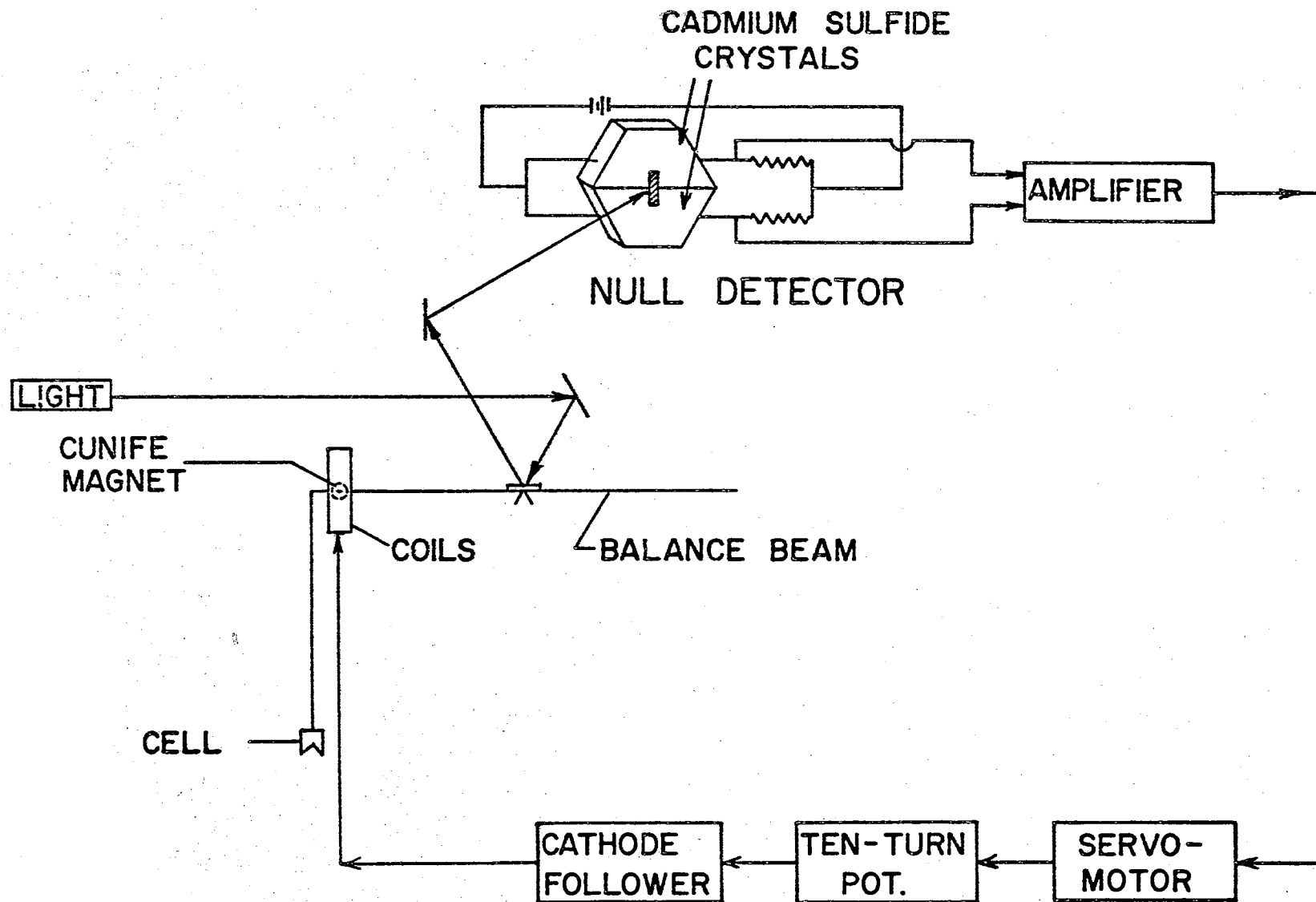
Figure 7. Automatic Control System I.
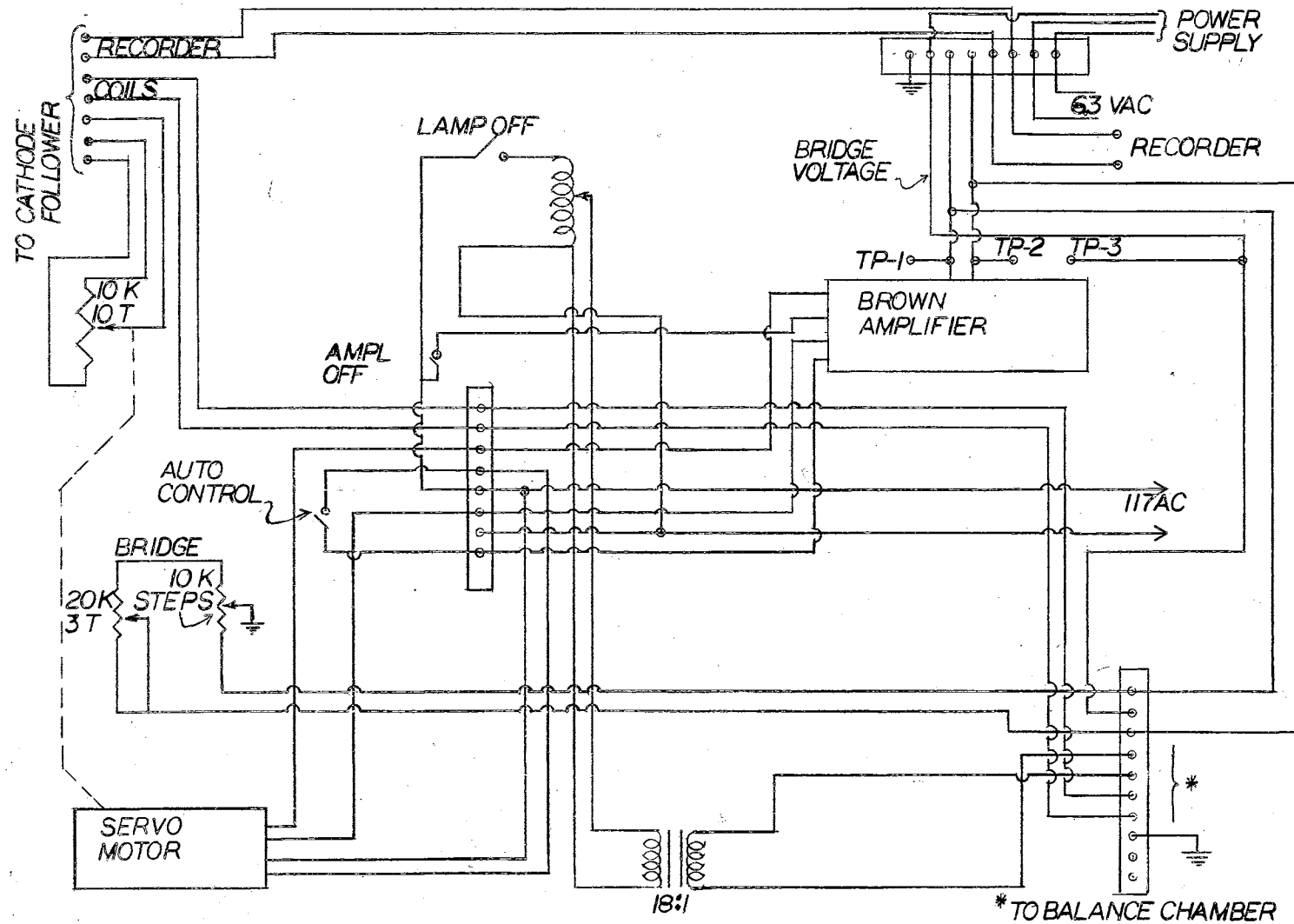
Figure 8. Schematic Diagram of Control System I.

certain features make it a new and outstanding device. Two strips of
metal are vacuum-deposited in parallel on a photoconductor (CdS). One
strip is so thin that its electrical resistance is quite high. This
corresponds to the resistance wire in ordinary potentiometers. The
other strip is relatively thick, and low in resistance. The brush
or contact wiper of the familiar potentiometer is replaced by a light
spot on the photoconductor in such a position that it bridges the gap
between the resistor strip and the conducting strip. The contact "wiper"
(light spot) obviously eliminates the brush wear and friction common to
mechanical potentiometers.

The role of the Photopot in System II is the same as that of the
cadmium sulfide crystals of System I. When employed in a Wheatstone
bridge circuit (Figures 9, 10), the full scan of the light spot on
Photopot produces a voltage output which varies from minus through null
to plus, and since the light spot position on the Photopot is determined
by the balance beam deflection, the result is an error output characterized
by a polarity and a magnitude. Several other advantages are obvious from
the manufacturer's description:

1. The sensitivity decreases strongly with decreasing light
    intensity for low load impedance. However, if the meter impedance
    is high ($\geq$ 1MΩ) the sensitivity is virtually independent of the
    light intensity.

2. For reasons intrinsic to the phonomenon of photoconduction
    and the impossibility of avoiding stray radiation, it is advisable
    for bridge circuit applications to work with as low a light inten-
    sity as practical and a high load impedance. In this way hardly
    any sensitivity is sacrificed for freedom from noise and drift
    stability.
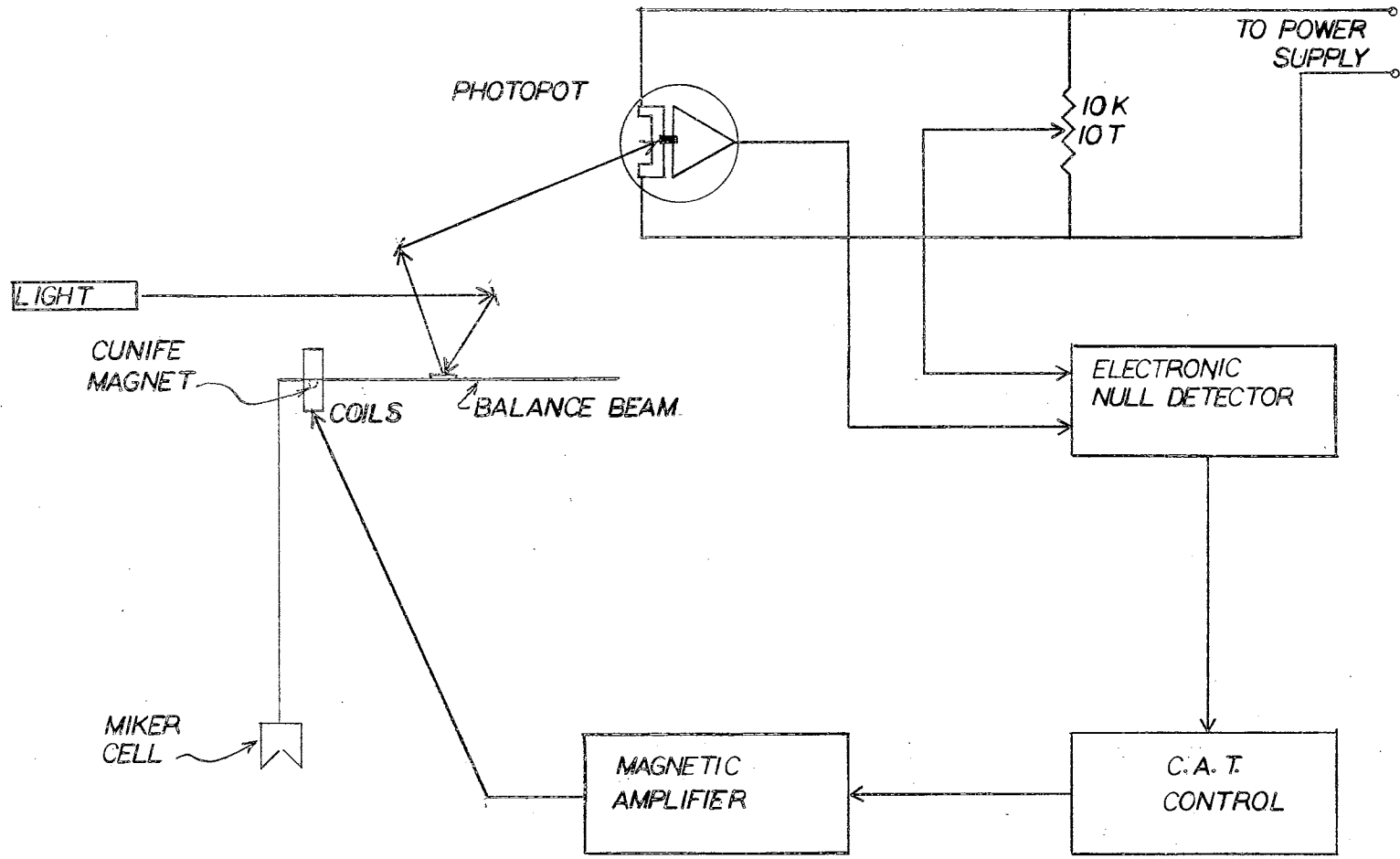
Figure 9. Automatic Control System II.
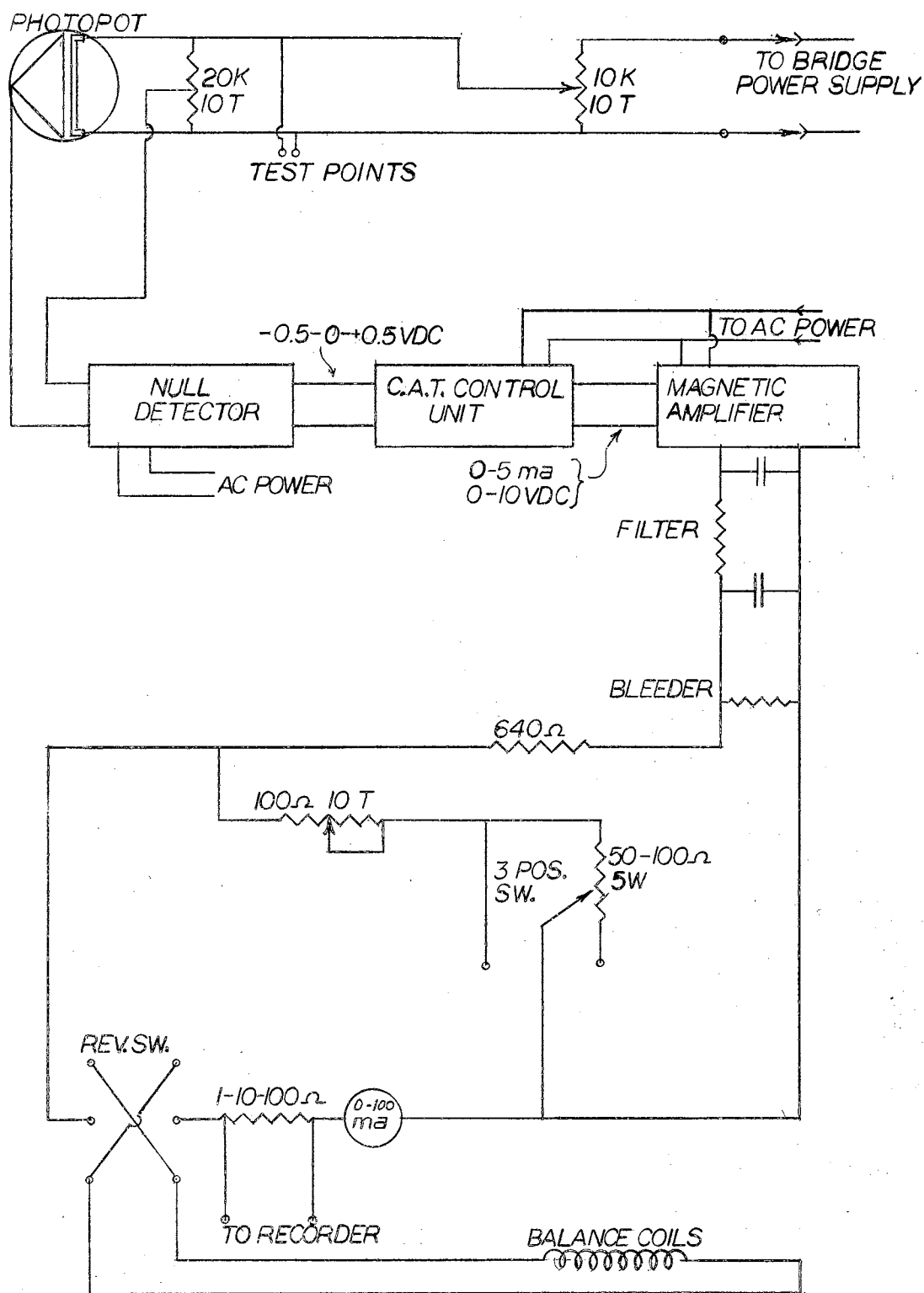
Figure 10. Schematic Diagram of Control System II.

3. If the bridge is used for null-seeking (servo) applications, linearity is of no consequence and sensitivity alone counts. With sufficiently high light levels, however, and with a load impedance of 1 MΩ or higher, the output voltage can be made linear with displacement about zero.

4. Stable zero readings in null-seeking applications can be obtained which are equivalent to better than 1 µ. It should be noted that further amplification can be realized simply by lengthening the light arm of the optical system.

The dc output of the bridge circuit is characterized by a magnitude and a polarity, both of which are determined by the position of the light spot on the Photopot. This comprises the dc error signal input to the Leeds and Northrup type 9834-2 electronic null detector.

The electronic null detector does three things:

1. The dc input signal is converted to ac; conversion is accomplished by a contact-vibrator. The converter contacts operate in synchronism with the line frequency.

2. The ac signal from $\underline{1}$, with magnitude and phase dependent on the magnitude and polarity, respectively, of the dc input signal, is amplified by four consecutive voltage stages employing conventional resistance-capacitance coupling. Provisions are made to protect the low level ac signals in the first two stages against the entrance of interferring voltages (noise), and to effectively ground transient voltages which enter the amplifier but which have frequencies higher than 60 cycles.

3. The amplified ac signal from $\underline{2}$ is converted to a dc output signal of magnitude (- 0.5 to + 0.5 volt) and polarity determined

by the magnitude and polarity of the <u>input</u> signal, <u>1</u>.

The output of the electronic null detector is the input to a Leeds and Northrup 10877, Series 60, Current-Adjusting Type (C.A.T.) Control System, which provides automatic corrective control action based on the magnitude, rate of change, and duration of the amplified error voltage. The C.A.T. unit is a voltage to current converter with a range of from <u>0</u> to <u>5</u> ma output. It provides three types of control action, each absolutely necessary for precise control:

1. Proportional action. This type of control makes the entire C.A.T. output (5 ma) available over an arbitrary band defined by the balance excursion. A setting of 10%, for example, will employ the entire C.A.T. output over a more narrow balance beam excursion than a setting of 50%. Regardless of the proportional band (10%, 50%, etc.), the control action is proportional to the error signal.[*]

2. Simple proportional action alone will not maintain the control point, but does provide the fast <u>response</u> required for close control. When reset action is superimposed upon proportional control, it provides recognition of control point which simple proportional control lacks. The reset action results in a change of the C.A.T. output at a rate proportional to the distance the balance beam is removed from the control point.

3. The third type of control is termed rate action. This corrective action varies the C.A.T. output in a manner proportion to

---

[*] One type of control system, perhaps more familiar to the reader, employs the C.A.T. unit (or equivalent) in conjunction with a recorder which serves as the control point indicator. By the proportional band is meant the per cent of full-scale recorder-pen excursion which is required to vary the C.A.T. output from minimum to maximum.

the velocity of the balance beam. Compensation of this type is sometimes referred to as error signal lead because it tends to offset the effects of measuring lags which would cause the balance to overshoot or oscillate about the control point.

A very important feature of the C.A.T. controller which has not been emphasized thus far is that it eliminates the need for a servo motor. In terms of a Miker cell losing weight by effusion this means that corrective current is applied and maintained as necessary to maintain the control point (just as though the servo motor were driving the ten-turn potentiometer of Control System I). Obvious advantages are the absence of gear slack which is inherent to some extent with even the most precise motor-gear trains, and the elimination of mechanical friction effects which, though small, produce measuring lags in the servo loop. Besides these advantages, the C.A.T. controller has a response time inherently less than that attainable with conventional servomotors.

The output of the C.A.T. controller (0 to 5 ma) could be used directly to energize the coils and drive the magnet on the balance beam, but this would provide a weighing range of only about 5 mg (Figure 17 and related discussion). Therefore amplification of the C.A.T. output is necessary. This is accomplished by making the 0 - 5 ma output of the C.A.T. unit the input to a Leeds and Northrup type 10910 magnetic amplifier which is equipped with adjustable load current feedback that controls the linearity, response time, and output. It should be emphasized that the magnetic amplifier is a current amplifier, and that the 5 ma input from the C.A.T. controller results in a nominal maximum of about 100 ma available to the coils.

The final link of the closed control loop, as described here, is the energizing of the coils and driving of the balance beam according to control point requirements (Photopot null-point).

Automatic Control. Considerable effort was spent in trying to achieve satisfactory control with Control System I. The chief source of difficulty evidently involved the null sensor, which did not produce an error signal proportional to the displacement of the light beam from null. Such a non-linear output is contrary to what was anticipated from the geometry of the CdS elements. A non-linear error signal results in an unstable servo loop, primarily because the balance is subjected to too large a corrective force when very close to null. The detector design is considered satisfactory; the source of difficulty appears to be in the constructional technique. This is evidenced by the fact that resistance values of about 1.5 and 0.8 megohms were measured across each crystal with only the polarity changed, which indicates that the contacts are not purely ohmic. Presumably, the source of difficulty is the CdS-In contact or the indium-conducting epoxy adhesive-copper contact. Only one such detector was tried and the nature of this difficulty was not pursued.

Control System II was installed near the end of this author's work. Consequently no systematic efforts were made to employ it under conditions of automatic control. Some preliminary work indicated that the system will be successful. A condition of rough control was attained in which the oscillations of the beam were confined to relatively small excursions. This is remarkable because no effort was made to optimize such variables as bridge voltage, proportional action, light intensity, error signal lead, or error signal lag. From these comments it is

obvious that no conclusion can be made at this time regarding automatic control of the present microbalance. Work continues on this problem, however, and will undoubtedly be reported by future workers.

Manual Control. Satisfactory manual control was realized for both control systems. With the first control system the ten-turn potentiometer was operated manually to control the balance position, as determined by aligning the pointer on the balance with the hair-line of a telemicroscope. The operator corresponds to the null detector for this type of control.

The Photopot and electronic null indicator (see Figure 9) were employed in manual control with the second control system. Manual adjustment of the current output of the C.A.T. unit served to control the position of the balance, as determined by observation of the null indicator. Manual control with this system has the advantage of eliminating the need for the telemicroscope. The operator can control the balance from arbitrarily remote distances.

Precision obtained is comparable for the two manual control methods. Ultimate precision should be greater for System II, however, because the sensitivity of the null indicator can be increased to exceed the magnification attainable with the telemicroscope.

Miker Cells. The majority of the experimental work was performed with graphite Miker cells (Figure 11). Cell variety was obtained by varying the angle T and the orifice diameter. The cells were con- structed from 0.5 in.-diameter graphite rod. The cell lid is threaded and screws into the cell body as indicated. No special difficulty was encountered in the construction of cells, but "good" threads were required as a safeguard against the possibility of leaks. The cell
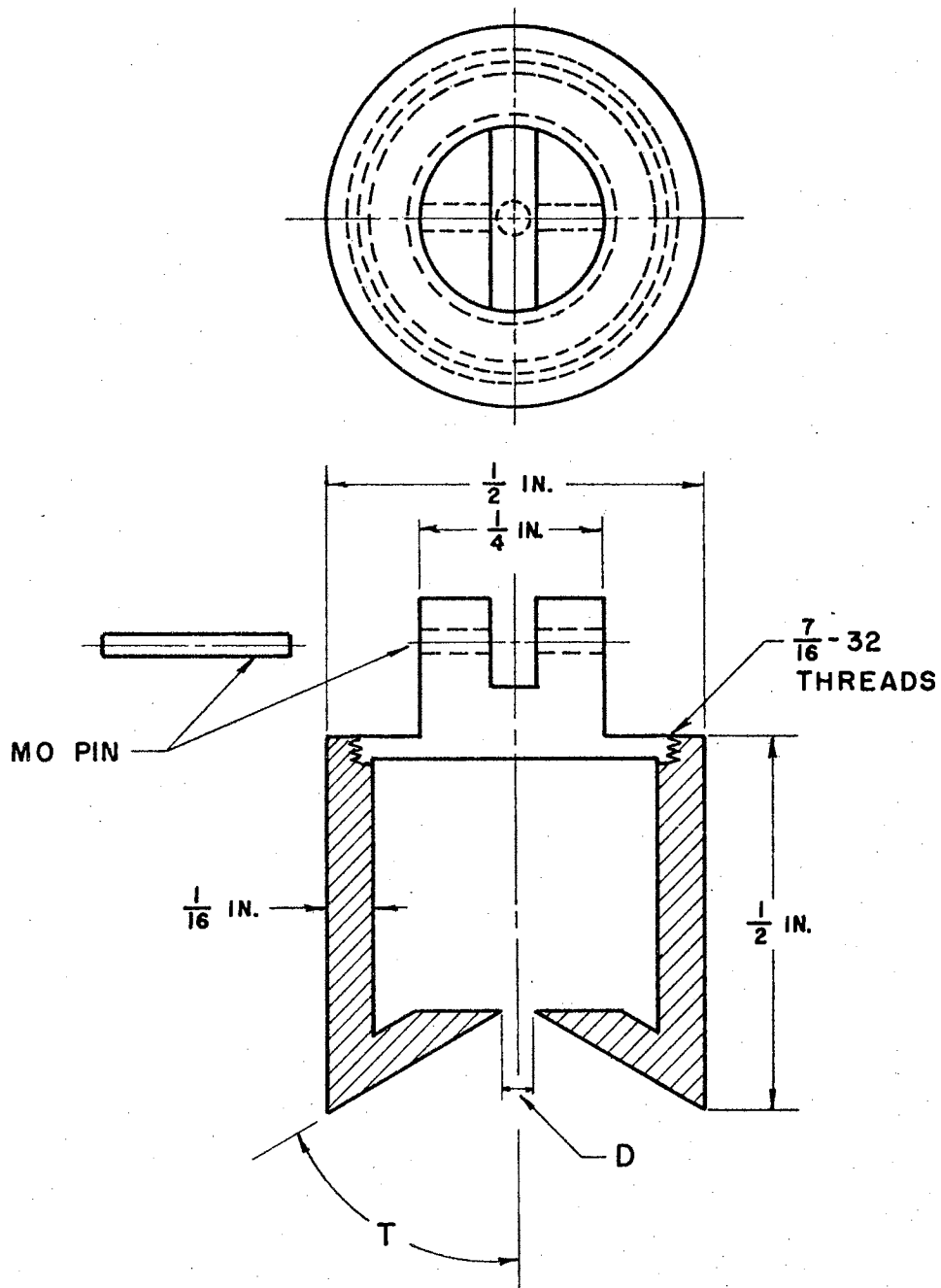
Figure 11. Miker Cell.

is attached to the balance suspension by a molybdenum hook which fits closely in the slotted section of the lid and is attached to a molybdenum pin inserted through the hole in the slotted section.

One quartz cell was employed; the design is basically the same as shown in Figure 11. A quartz tube was sealed at one end and suction was applied while the end was soft to draw the softened quartz into the tube; angle $\underline{T}$ results. The orifice was then drilled with a water-cooled tungsten rod. The other end was then sealed, and simultaneously a small hook for attachment to the balance suspension was pulled. This technique is not recommended for producing satisfactory Miker cells; the precision is rather poor. Angle $\underline{T}$ cannot be constructed accurately; the angle which results must be accepted. Several breakages occurred in the drilling of the orifice. In cases where the inertness and high temperature characteristics of quartz (or fused silica) are particulary important, however, these disadvantages become less important.

The parameters for all Miker cells employed in this work are given in Table II.

The Furnace. The heating element, Figure 12, is a modification of one employed by Blakelock and Machin[5]; it is a hollow graphite cylinder with 4-in. length, 1.5-in. o.d., and 1.1-in. o.d. Longitudinal slits are spaced at 45° intervals around the element to produce the desired electrical resistance. The slits extend to within 0.25 in. of the top and bottom of the element. The current flows through a graphite section approximately 0.2 in. thick and 0.4 in. wide except at the ends, where the section is about 0.25 in. wide. The constriction provides increased resistance, and therefore increased power input per unit length of current path, thereby compensating for the greater heat dissipation

TABLE II

PARAMETERS OF MIKER CELLS

Cell	Used For	Orifice Parameters[a]			Correction Factors[b]	
		L, in.	D, in.	T, deg.	W	F
1	Ag	0.127	0.059	60	0.996	1.12
2	Sn	0.209	0.082	45	0.975	1.16
3	CaF_2	0.127	0.0635	60	0.996	1.12
4[c]	Ag	0.188	0.074	63	1.00	1.12
5	Au	0.120	0.053	60	0.996	1.11

[a]L = length, D = smallest diameter, T = off-axis angle.

[b]Interpolated from Table I.

[c]Quartz cell, all others graphite.
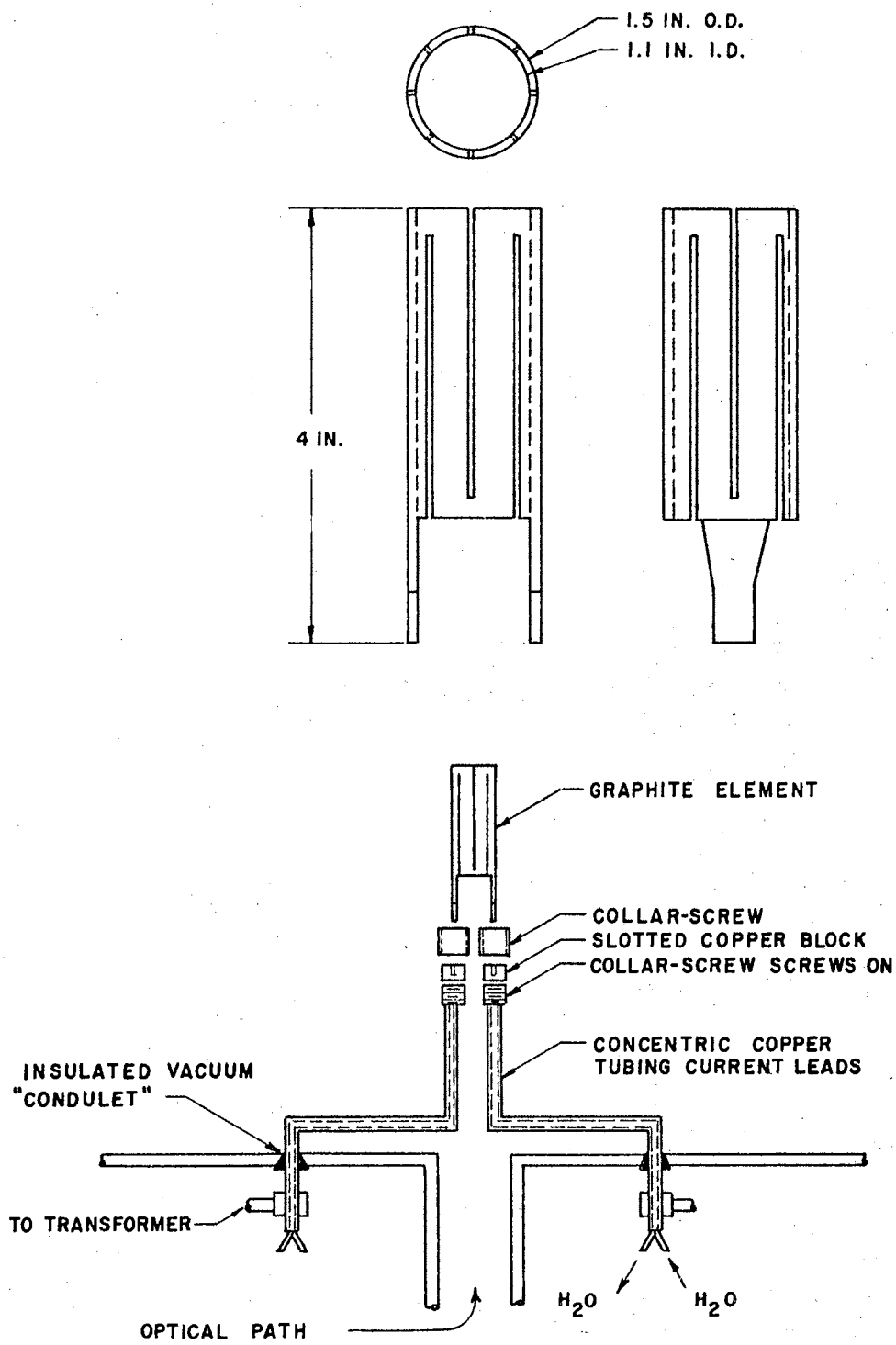
Figure 12. The Heating Element.

from the end regions. The resulting thermal profile (temperature vs. position on heating element axis) will therefore have a flatter maximum, i.e., a longer isothermal region, than it would without this compensation. The heating element is surrounded by a single-thickness, cylindrical radiation shield (not shown). Both molybdenum and tantalum were employed as shielding materials.

The slits in the heating element provide as a bonus an extremely desirable feature. The current path through the heating element is effectively that of a non-inductive winding; hence, any inductive effects, which might interact with the Miker cell, are cancelled.

The two legs of the heating element fit tightly into rectangular slots milled in solid copper cylinders. The cylinders rest on threaded brass plugs and are firmly held by threaded collars which screw onto the brass plugs. This arrangement allows small "x-y" adjustments of alignment of the heating element. Each brass plug is silver-soldered to a 0.5-in.-diameter copper tube, through which cooling water flows to the plug; the cooling water flows out through a 0.25-in. copper tube which is inside the 0.5-in. tube. The water-cooled copper tubes also serve as electrical lead-ins through which low voltage ac power is supplied.

Electrically insultated connections through the vacuum chamber wall are achieved by means of Condulet connectors (Crouse-Hinds Co., Syracuse 1, New York) as indicated. The "Condulet" connectors also allow radial and vertical adjustment of the heating element. Outside the vacuum chamber insulated copper cable (size 500 MCM) connects the copper tubes with the transformer; polyethylene tubing is attached to the copper tubing to achieve electrical insulation from the water and drain lines.

Special caution is necessary to avoid exerting a mechanical strain
on the heating element; forces which arise from the stiffness and weight
of the cable may be exerted at the external cable connections and trans-
mitted to the heating element through the rubber Condulet bushings. The
transformer cables are therefore supported independently (not shown).

Initially it was not known whether the electrical contact between
the heating element and the water cooled terminals would be adequate.
After short usage, however, the legs of the heating element were
observed to be bonded inseparably to the slotted copper terminals. In
fact the entire assembly was "frozen," including the threaded collar.
This was considered beneficial because good electrical contact was
assured. The heating element was operated for a total of several hun-
dred hours at temperatures up to $1500^{\circ}C$. At the end of this period,
there was no discernible deterioration.

The heating power is adjusted by a 220v Variac which controls the
input to the 4 Kva, 6/8/10v transformer. No special voltage regulator
was employed.

The Vacuum System. The main features of the vacuum system appear
in Figure 13. Basically the system consists of a furnace chamber, a
balance chamber, and connecting tubing. The position of the heating
element is shown for clarity. The balance chamber was constructed from
brass tubing 12 in. in length, 6 in. i.d., and 6.5 in. o.d.; flanges
with O-ring grooves are silver soldered to each end. The ends are 0.38-in.
brass plates and are secured to the balance chamber flanges by bolts.
Each end plate has a port window of rather common design -- a quartz
disc, 2 in. in diameter and 0.25 in. thick, is pressed against a rubber
O-ring mounted in an O-ring groove. There is a similar port window in

BALANCE CHAMBER ON
FELT LINED MAPLE CRADLE
(NOT SHOWN)

PORT
WINDOW

VMB-I

ELECTRICAL
LEAD-INS

AL BLOCK TO
PREVENT COLLAPSE
OF BELLOWS

BELLOWS

1/2 IN. O.D. CU TUBING

"CENCO" VACUUM CONNECTOR

O-RING
CONNECTION

FURNACE
CHAMBER

RACK

"CONDULET" CONNECTOR

TO TRANSFORMER

PERISCOPE FOR
PYROMETER SIGHTINGS

TO CONCRETE
FLOOR

TO BAFFLE, DIFFUSION PUMP,
AND MECHANICAL PUMP
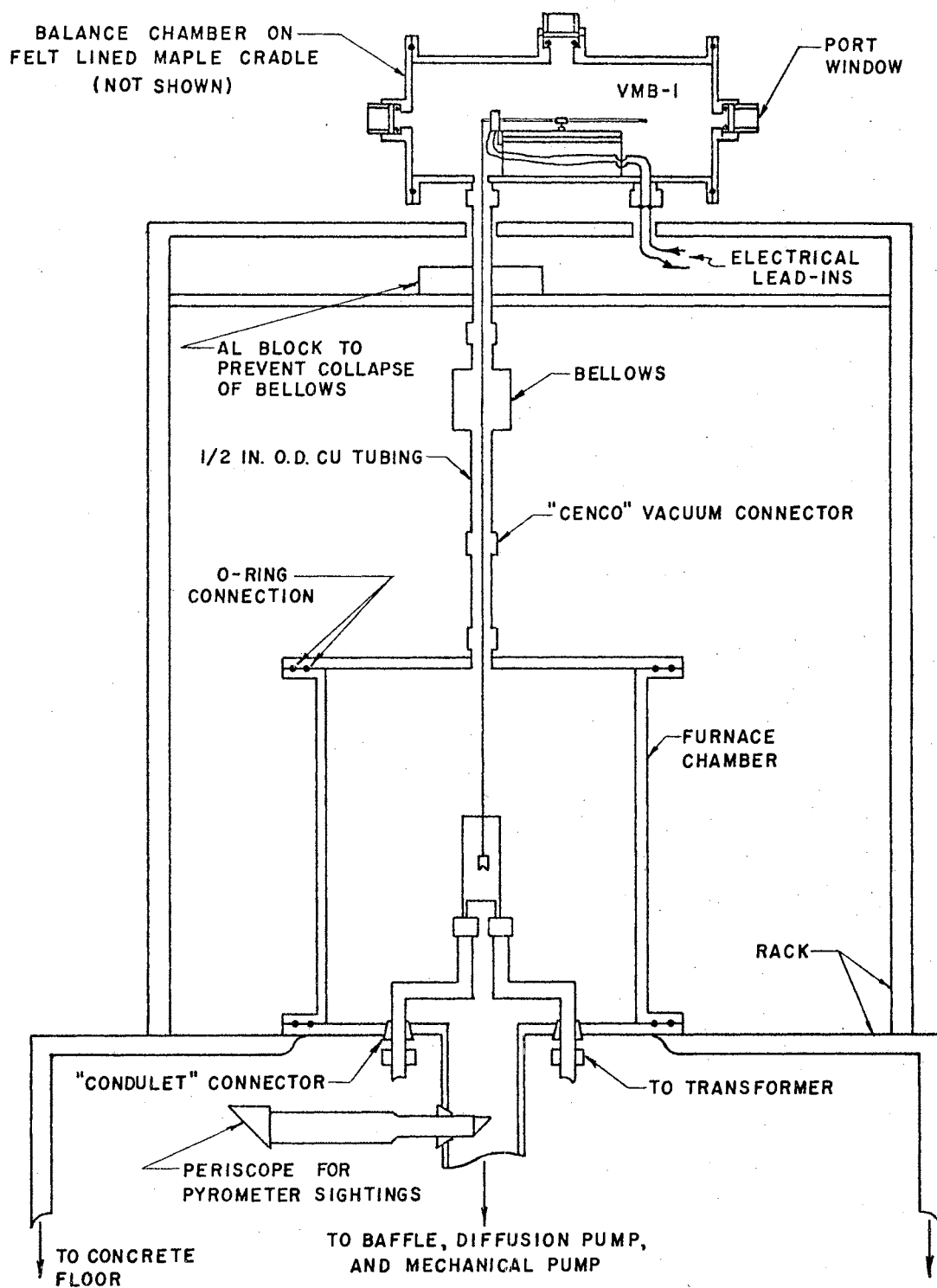
Figure 13. The Vacuum System.

the top of the chamber. The port windows at the ends permit observation of the balance. The one at the top transmits a light beam to and from the mirror on the balance beam. Two connections are made at the bottom of the chamber with Cenco vacuum connectors: one of these is for the tubing which connects the balance chamber to the furnace chamber; the other is for current lead-ins. A vacuum tight, insulated lead-in (a multi-pin header) was soldered into a hole drilled in the cap of a Cenco connector to provide terminals for connecting the current leads inside the balance chamber to those outside.

The balance chamber is seated in a felt-lined maple cradle, which rests on a table constructed from angle iron and 0.75-in. plywood.

The vacuum connection between the two vacuum chambers consists of three sections which are coupled with Cenco vacuum connectors. The middle section is a flexible brass bellows which not only absorbs vibrations but also provides an entrance to the furnace chamber for transferring cells. Disconnection of the Cenco connector which couples the furnace chamber lid to the connecting tube permits the bellows to be collapsed, which provides working room to make or break the hook connection in the balance suspension.

The furnace chamber is a 12-in. length of 12-in. diameter cold-rolled steel pipe, copper-plated to decrease porosity and corrosion. Flanges are welded onto the ends of the chamber; the upper flange contains O-ring grooves which provide a vacuum seal with the lid. The chamber rests on a copper plated steel base which contains O-ring grooves. Steel rods 0.25 in. in diameter, are mounted on the base plate, and provide a lattice for constructing radiation shielding about the heating element. Cooling water is conducted through copper tubing

soldered to the top, sides, and bottom of the furnace chamber.

The water-cooled current leads enter the chamber via Condulet connections in the base plate. A 4-in. diameter outlet at the center of the base plate makes connection to the pumping system, which consists of a water-cooled baffle and a consolidated MCF oil diffusion pump backed by a Welch Duo Seal mechanical pump. The mechanical pump was connected to the diffusion pump by 2-in. diameter rubber tubing, which was found to be an excellent vibration absorber. A stout cord connected tautly from the middle of the rubber tubing to the steel frame which supports the entire system improved the damping of vibrations from the mechanical pump.

Temperature Measurement. Pyrometer sightings directly into the Miker cell are highly desirable for the Miker cell serves as an excellent black body, and emissivity corrections are unnecessary.

A periscope arrangement, constructed to permit pyrometer sightings directly into the Miker cell, appears in Figure 14. A right-angle prism is attached by epoxy adhesive to each end of a Pyrex tube. The vacuum connection is a large Condulet connector. The inner prism is protected from effusing vapors, except during pyrometer sightings, by a cylindrical shield fashioned from 0.001-in. thick tantalum sheet. The shield is attached to beryllium-copper tubing which has a Cunife magnet soldered to one end. The tubing is contained in the Pyrex tube and can be moved by means of the external magnet as indicated. This device operated satisfactorily.

A Leeds and Northrup Model 8622-C pyrometer was employed. This instrument was compared frequently via a tungsten strip lamp to a like model certified by the National Bureau of Standards. The two instruments

OPTICAL
PYROMETER

MIKER CELL
ORIFICE

TANTALUM
SHIELD

PYREX TUBE

NEOPRENE BUSHING FOR
CONDULET VACUUM CONNECTOR

MAGNETS (OPERATE SHIELD)
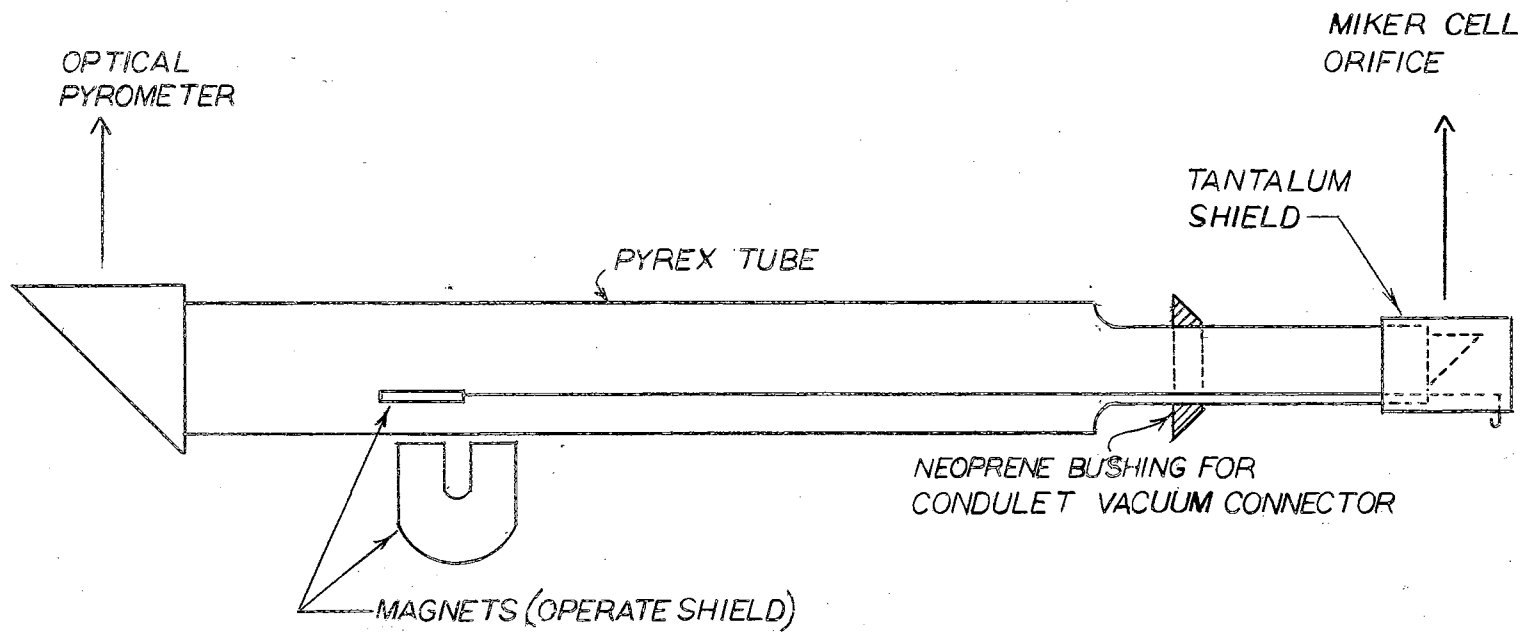
Figure 14. Prism Arrangement for Pyrometric Sightings into the Miker Cell Orifice.

gave identical readings to the nearest scale division (within $5^{o}C$) each time they were compared.

It is essential that the periscope be mounted so that the view through the optical pyrometer follows a right angle path. Otherwise, distortion occurs which changes the apparent brightness of the Miker cell orifice and results in erroneous temperature measurements. The temperature as measured by pyrometer sightings through the prism arrangement was 40° lower than when measured without the prisms.

CHAPTER IV

EXPERIMENTAL PROCEDURE AND RESULTS

Microbalance Calibration. The microbalance was calibrated with a

set of weights which were made by cutting suitable lengths of small-

diameter tungsten wire. The mass of the individual calibrating weights

was determined to ±0.02 mg with a Sartorius-Werke semi-microbalance.

The calibration procedure consisted of adjusting the current through the

coils to bring the balance beam to null position, adding a calibrating

weight, and readjusting the current to return the beam to null. The

coil current was adjusted by manual operation of the ten-turn potentio-

meter (Figure 7); balance beam position was observed with a Gaertner

telemicroscope.

The anticipated source of largest error was possible unknown shifts

of null point, which might be caused by inadvertent mechanical disturbance

of the balance during addition or removal of a weight. It was therefore

required, as a condition for satisfactory calibration, that the initial

null point be reproduced after each weight was employed.

The results of the calibration are given in Table III; the plot

of these data in Figure 15 shows the relation between suspended mass and

coil current to be linear over the available current range. The slope

of the calibration curve in Figure 15 is 0.289 mg/ma. A least squares

determination of the slope from the data in Table III gives a value of

0.2883 mg/ma. The solid circles in Figure 15 were determined after the

TABLE III

CALIBRATION DATA FOR MICROBALANCE

Mass of Wire Weight, mg	Compensating Current Through Coils, ma
0.40	1.983
0.87	3.530
1.13	4.488
2.01	7.680
3.64	12.502
5.09	18.600
6.20	22.180
7.49	26.516
8.89	31.940
9.41	34.044
15.83	56.25
18.02	63.12
19.85	69.20
21.66	75.26
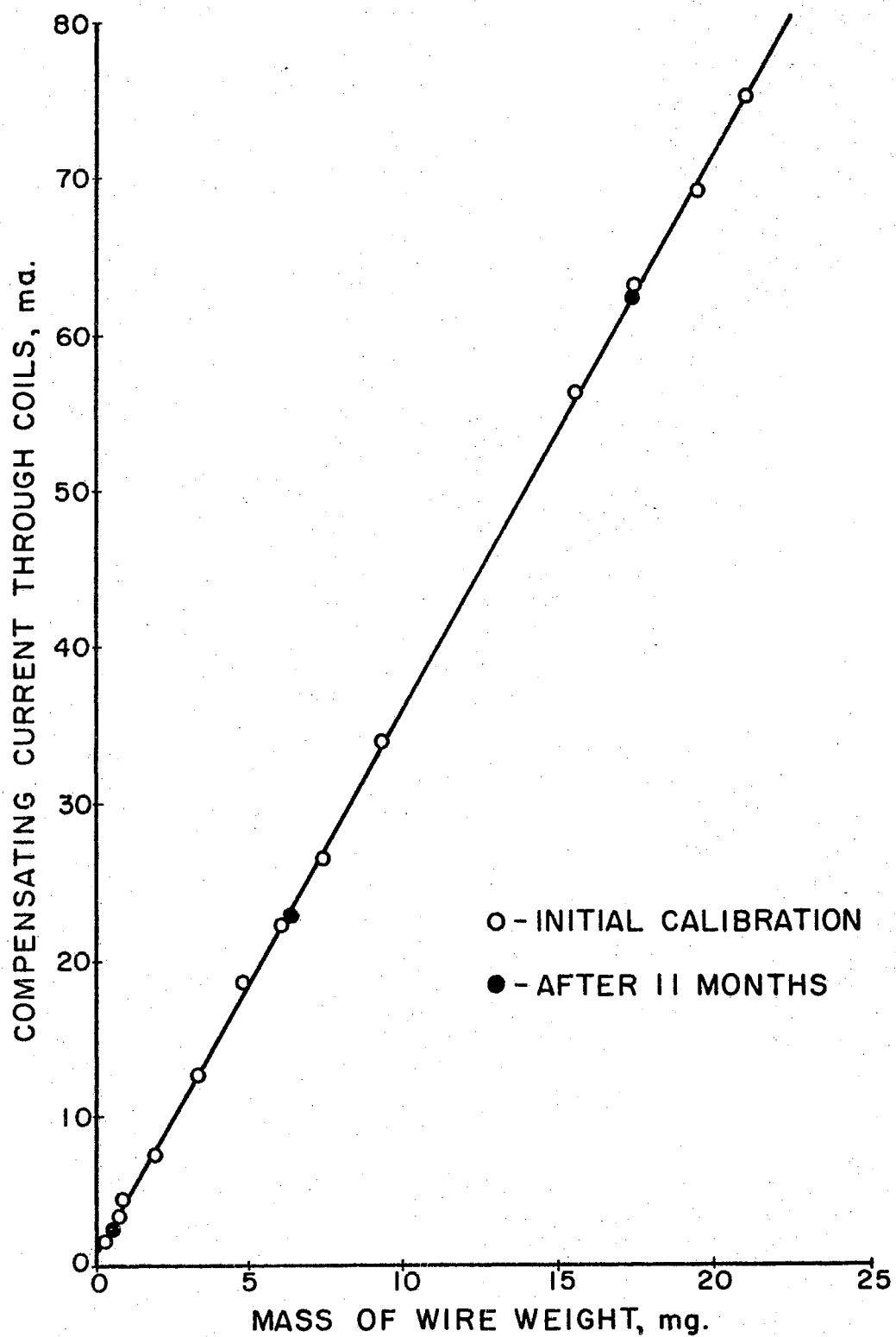
Figure 15. Microbalance Calibration Curve.

microbalance had been in operation for eleven months.

A graduated reticle in the eyepiece of the telemicroscope was calibrated with the result: 1 scale division = 120 μa x 0.289 μg/μa = 33.6 μg. The smallest beam displacement readily detectable with the telemicroscope corresponds to about 0.1 scale division or about 3.4 μg. The resolution of the balance must therefore be considered as about ± 4 μg, but it should be emphasized that this figure is a direct result of the use of a rather low-powered (approx. 30x) telemicroscope, and that automatic control coupled with photodetection of beam motion should improve the resolution by at least a factor of ten.

Bouyancy Effects. The effect of bouyancy is readily calculated. The calibration data yield

$$I = cm', \tag{32}$$

in which I is the coil current which compensates for a given wire weight of apparent mass m', and c is the slope. The apparent mass m' is related to the actual mass m by

$$m' = m - m\, \rho_a/\rho_w, \tag{33}$$

in which ρ_a is the density of air (0.0012 g/cm^3 at 20°C and 760 torr[31]), and ρ_w is the density of the wire weight (8.92 g/cm^3 for copper at S.T.P.[31]). Substitution of (33) into (32) yields

$$I = cm - cm\, \rho_a/\rho_w, \tag{34}$$

or with values for c and ρ_a/ρ_w inserted,

$$I = 0.2883\, m - 3.90 \times 10^{-5}\, m.$$

It follows that bouyancy effects are negligible. Furthermore, any constant asymmetric bouyancy effects present during calibration in air and which are then removed during operation in vacuum do not influence the calibration, but merely shift the zero-point of the mass vs. current curve.

Some tungsten wires were employed as calibrating weights, but the density of tungsten (19.3 g/cm^3) is greater than that of copper, and the bouyancy effects, as calculated above, are proportionally less.

Weighing Range of VMB-1. From the available current range of about 80 ma, it is apparent that mass changes totaling about 23 mg can be determined. The available range, however, is actually twice this value, or about 46 mg, because the polarity of the coil current can be reversed. It is possible to begin a series of runs with maximum cur-rent, about +80 ma, so that null compensation entails a decrease in the coil current; then, when the coil current is decreased to zero, the polarity is reversed and the series of runs continued until the other end of the current range (approx. - 80 ma) is exhausted. Once the full 160 ma (approx.) is exhausted in this manner, the balance is retared by opening the off-sample side of the balance chamber and adding or substracting tare wires as necessary. This simple operation makes the entire current range available again, and determinations are con-tinued without disturbing the cell.

General Operating Procedure. All cells, before being charged with sample, were heated to constant weight at about 1500°C. The pressure of the furnace chamber was usually about 1 x 10^{-6} torr during heating. A pressure of 5 x 10^{-5} torr was selected as the furnace pressure above which no heating was performed. A simultaneous determination of the pressure in the balance chamber showed that in the early stages of pumping it lagged almost exactly one order of magnitude behind the pressure in the furnace chamber and on extended pumping slowly approached that of the furnace chamber.

After the preliminary heating, the empty cell was removed from the vacuum system, charged with sample material, and returned to the vacuum system. The balance tare was then adjusted to provide an adequate current range. Each new sample was heated for a short period at temperatures higher than the experimental range of interest.

No special treatment was employed on the various samples; the following specifications are given by the suppliers:

Sn   99.99% Lot No. 1537 (Baker)

Ag   99.97% Lot No. 791231 (Fisher)

Au   99.95(+)% (J. E. Bishop)

CaF_2 99.994% Lot No. 771004 (Fisher)

The coil current was recorded continuously with a Sargent Model MR Recorder. To obtain a null reading, the coil current was increased in a direction which caused the beam to approach null as effusion occurred. At the instant the beam was at null, the standardization button on the recorder was depressed. This produced a spike on the recorder tracing, and, since the chart speed was known, recorded both the current and the time of the null. The coil current was then again increased as before and the procedure repeated. In this manner a series of spikes were obtained for each run which provides a plot of current vs. time and therefore of mass vs. time (0.288 mg/ma). During the entire procedure the balance beam never touched the rest stops.

Pyrometer sightings were taken intermittently during a run. At no time was the temperature observed to fluctuate from its initial steady state value; the straight lines obtained from a plot of coil current vs. time give direct confirmation of constant temperature conditions.

At the instant of recording the last null determination, a switch

was thrown which de-energized the heating element. After the disappearance of the recoil effect, the coil current was adjusted to return the beam to null and was recorded on the recorder chart paper along with the other data.

Auxiliary Determinations. Several questions are of immediate interest regarding the practicality of the Miker technique:

1. Is there a serious empty-cell recoil analogous to that observed by Bader[1]?

2. Does the heated cell interact in a spurious manner with the heating element as did the induction-heated torsion system of Searcy and Freeman[53]?

3. Do serious temperature gradients exist in the Miker cell?

4. For graphite cells with metal samples, is permeation[11] of the graphite cell walls by the metal vapors a problem?

5. Does significant surface diffusion[64] occur?

6. As effusion continues, is there a minimum sample size which must be present in order to obtain equilibrium pressure determinations?

The results of some determinations which give information concerning these and other questions appear in the following sections. Also included are results for a sample-blocked orifice and for limiting rate of effusion determinations.

Empty Cell Behavior. Initial testing of the apparatus and the Miker technique was made with a graphite cell containing silver. The values obtained in the first five runs for the molecular weight of silver were: 6.8, 2.5, 22, 146, 104. When an empty cell was substituted for the one containing silver, the apparent recoil forces, as

measured by the apparent difference in weight of the cell when hot ($1200^{\circ}C$) and when cool ($400^{\circ}C$), were quite erratic, but did exhibit a trend with temperature. These apparent recoil forces for empty cells were eliminated by removing a molybdenum disc (radiation shield) which had been attached to the balance suspension wire about 2 in. above the heating element. The spurious recoil forces for empty cells apparently resulted from a radiometer-type effect (the bottom of the molybdenum disc was exposed to radiation from the furnace and was therefore hotter than the top surface), or from a larger number of molecules, with a higher average speed, arriving at the bottom of the disc from the furnace volume, as compared with those arriving at the top of the disc from the cool walls of the vacuum chamber.

After the molybdenum disc was removed from the suspension wire, an empty cell was again tested for a recoil effect. Within the resolution of the telemicroscope ($\pm$ 4 μg), no recoil force was detected. This observation was repeated with other cells at temperatures up to about $1500^{\circ}C$. Furthermore, no observable balance motion occurred during the sequence: (1) balance initially at the null point with a degassed, empty cell suspended into the furnace at a temperature of $1300^{\circ}C$; (2) a switch was thrown to de-energize the furnace; (3) the furnace and cell cooled for several minutes; (4) the switch was operated to re-energize the furnace; (5) the furnace and cell return to the original temperature. It therefore appears that the spurious recoil forces have indeed been eliminated, and that interactions between the cell and the heating element, as reported by Searcy and Freeman[53], Shear[54], and Bader[1], are not present in this apparatus.

Typical Run. Typical of the majority of determinations is CaF_2

Run No. 9, data for which appear in Figure 16. Each point on the curve

represents a null determination. In this case, as for most, the rate

of effusion can be obtained precisely from only the initial and final

null determinations. But in all cases, as a safeguard against pos-

sible erroneous null determinations and temperature flucuations, several

null determinations were performed.

The slope of the curve in Figure 16 yields 6.127 µg/sec as the

rate of effusion, and, since this is a typical result, no special com-

ment applies. In some runs which were begun before a constant tem-

perature was attained, the early part of the cooling curve shows clearly

the change in the rate of effusion with temperature, i.e., $d(dg/dt)/dT$.

Fast Runs. At temperatures sufficiently high to produce pressures

approaching the transition region, which represents the upper pressure

limit of validity of the Knudsen equation, difficulty might be expected

in providing compensating current fast enough to monitor the effusion

and yet retain accurate null determinations. This would be expected

to apply particularly under conditions of manual control. Often the

problem of too rapid effusion is eliminated in conventional Knudsen

determinations by employing cells with appropiately smaller orifices

for the higher temperature ranges. But the convenience and superior

experimental technique of using one cell for an uninterrupted series

of runs which spans the entire Knudsen range is very appealing. For

this reason some runs were made to determine the maximum limiting rate

(µg/sec) accessible under conditions of manual control. Figure 17

shows the results for Ag Run No. 14 at 1458°K for which the rate of

effusion is 32.2 µg/sec. This corresponds to a vapor pressure of

2.1×10^{-4} atm which approaches the transition region. With the same
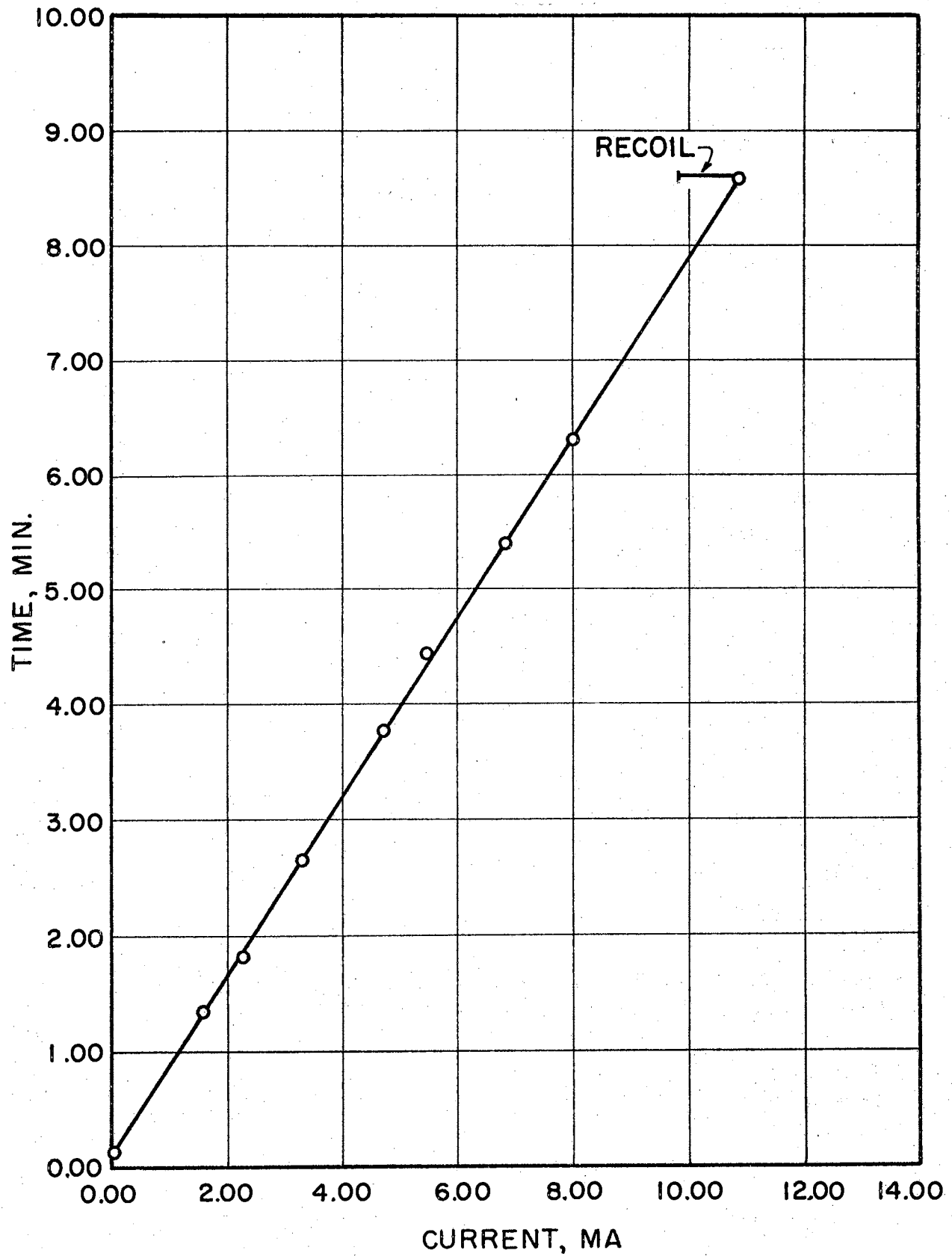
Figure 16. Typical Experimental Data-Calcium Fluoride, Run 9.
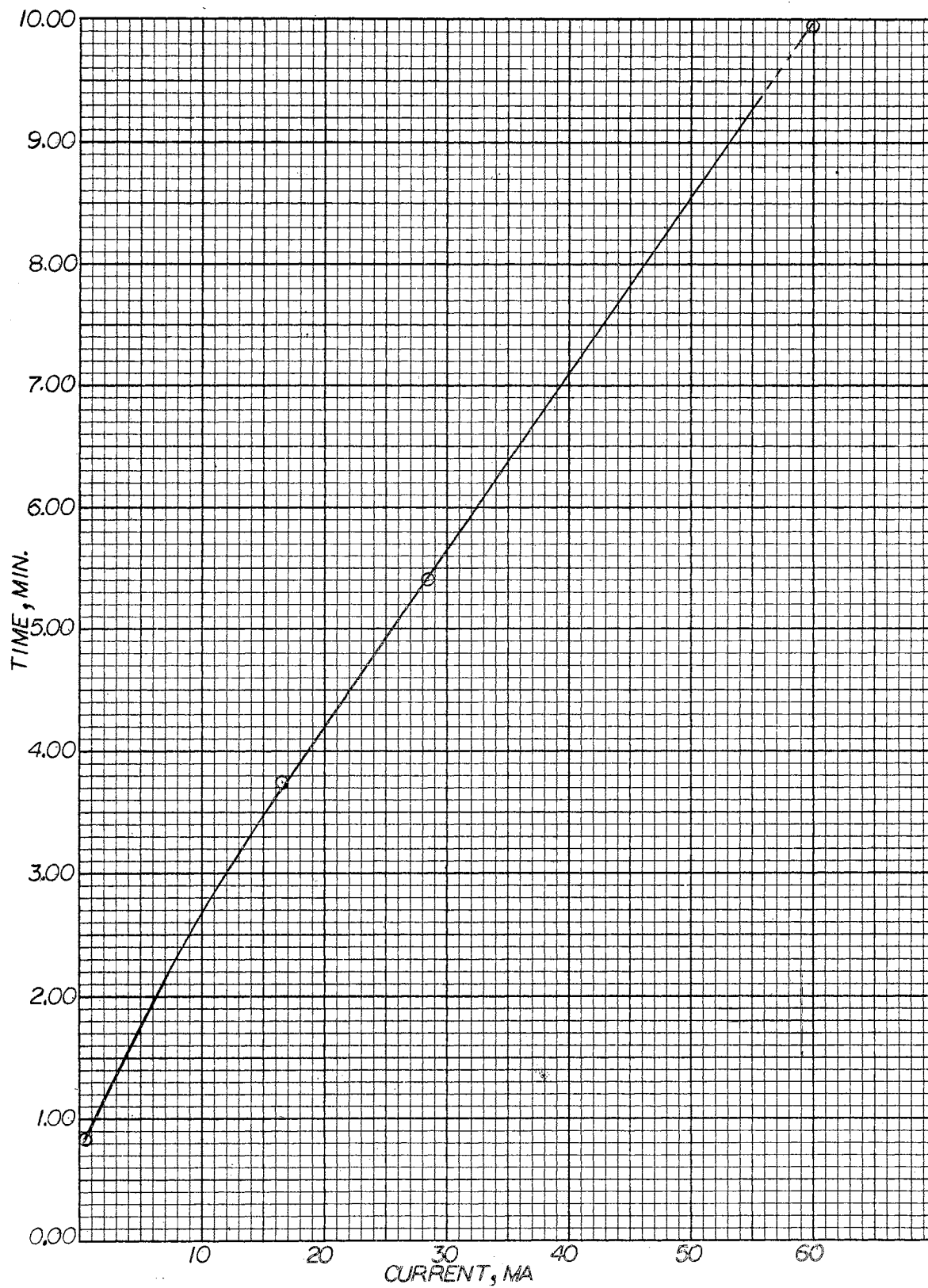
Figure 17. Rapid Effusion - Silver, Run 14.

cell, an effusion rate of 0.051 μg/sec was measured for Ag at 1150^OK. The latter rate yields a pressure of 2.8 x 10^{-7} atm.

Though reliable rates of effusion can be determined for the rapid effusion, a rather serious error arises for the measurement of the recoil force. The null determinations may be described as "running" nulls because the instant at which the balance beam reaches null is recorded. Consequently, if the balance is moving rapidly, as for rapid effusion, an appreciable overshoot of the null results. This is not objectionable for the rate of effusion determination; no error is intro-duced by the overshoot so long as each null is determined in the same manner. But the last null is accompanied by de-energizing of the heating element and the recoil force is measured by the current required to return the balance to null. Thus the overshoot occurs in a direction which reduces the observed recoil force. For slower effusion the balance either approaches null very slowly, or can be impeded by adjusting the compensating current, and no such problem arises. But for rapid ef-fusion, it becomes a question of the skill of the operator and his ability to impede the rate of approach to null so as to eliminate or minimize the final overshoot.

Underloaded Cell. The effect of diminishing sample on the rate of effusion is shown in Figure 18. Results for CaF_2 and Au are compared when the surface area of each sample was about the same as the area of the orifice.

A large sample-surface-area to orifice-area ratio is desirable. The minimum value of this ratio which still assures equilibrium pressure depends on the evaporation coefficient of the sample substance. For similar surface areas, the rate of effusion of Au maintains its equilibrium
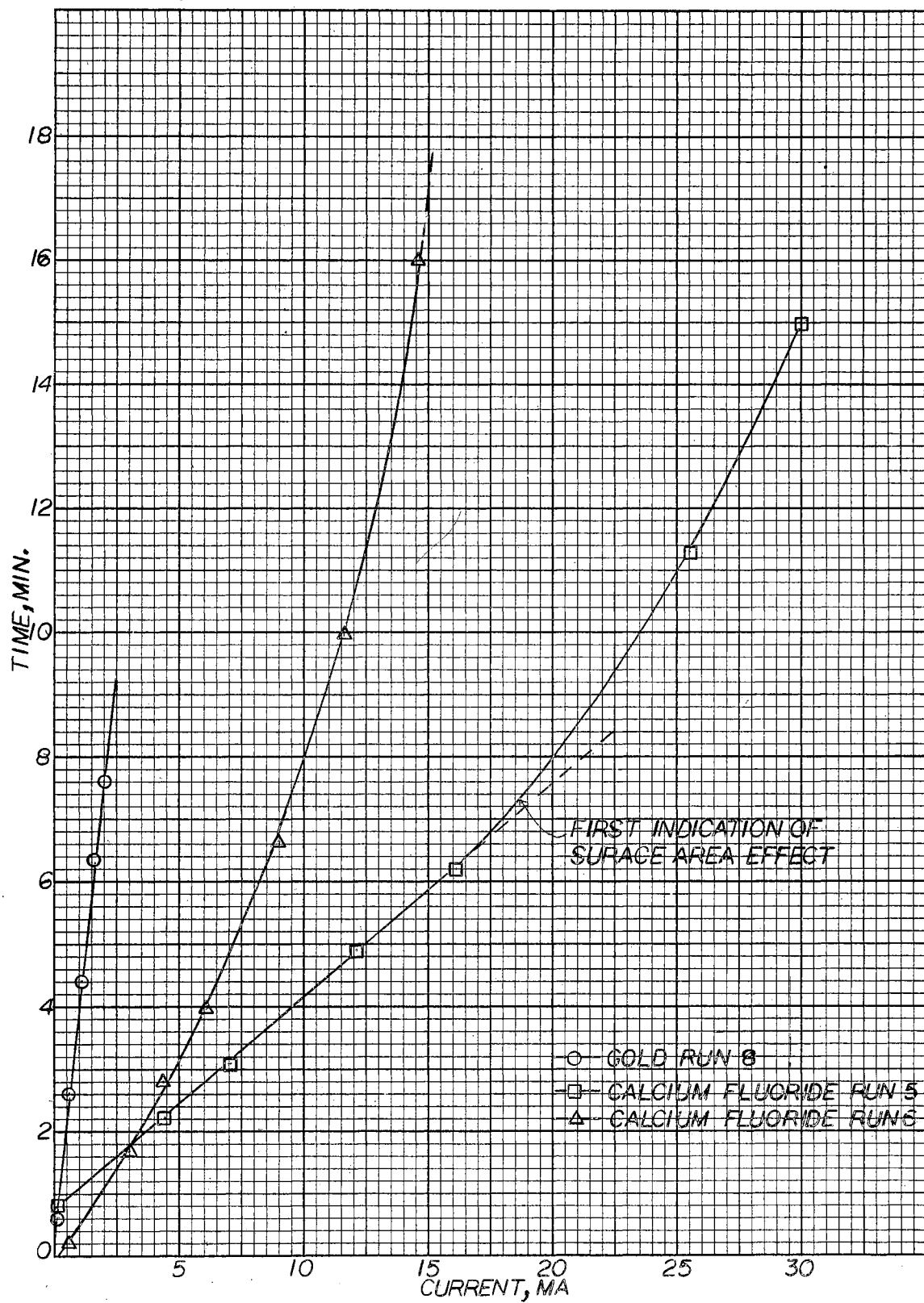
Figure 18. The Effect of Diminishing Sample-Surface-Area on the Rate of Effusion.

value while that of CaF_2 begins to decrease; this indicates the evapora-
tion coefficient of Au to be nearer unity than that of CaF_2. If $\underline{s}$
represents the surface area of the sample, then the results in Figure 18
yield $d(dg/dt)/ds$. Effusion rate determinations for calculation of P_K
require that this quantity be zero; for which a necessary and sufficient
condition is that a plot of g vs. t be linear.

Sample-Blocked Orifice. A cell was packed with CaF_2 so that the
orifice was blocked and effusion occurred directly from the sample sur-
face. Table IV presents data for seventeen runs which were made with
the cell loaded in this manner. Effusion rate determinations were made
above and below the melting point of CaF_2 ($1633^{\circ}K$); the cell orifice
remained blocked by the molten CaF_2. Such an arrangement corresponds
to a pseudo-Langmuir[43] type determination, and presumably the results
could be interpreted as such, though no effort was made to do so. The
interest here was with effects which might result should the orifice
become blocked in the course of normal Miker determinations.

If the pressures $\underline{P}_K$ and $\underline{P}_R$ are expressed in terms of the Clapeyron[64]
equation,

$$\ln P_K = - A/T + B, \tag{35}$$

and
$$\ln P_R = - A'/T + B', \tag{36}$$

then we may write

$$\ln (P_K/P_R) = \frac{- A' - A}{T} + B - B' \tag{37}$$

Ideally, $P_K = P_R$, and therefore a plot of $\ln (P_K/P_R)$ vs. $1/T$ should
be a straight line with ordinate value of zero at all values of T.

Figure 19 compares $\underline{P}_K/\underline{P}_R$ for a normal cell to that of the over-
loaded cell. The $\underline{P}_K$ values for the two cells are in good agreement,
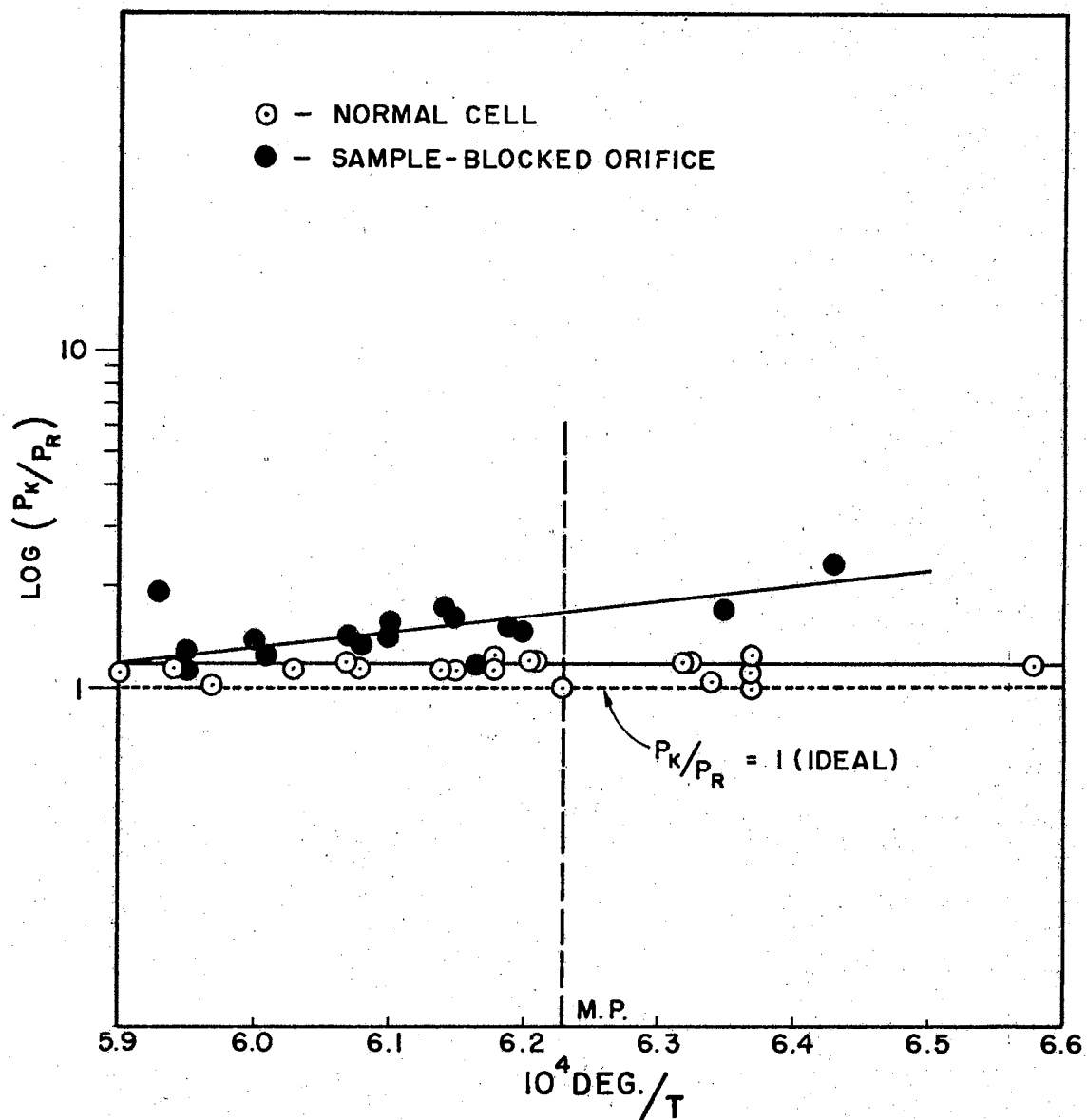
Figure 19. The Blocked-Orifice Effect, from Calcium Fluoride Data, Table IV.

although with only three exceptions the ones for the overloaded cell are slightly lower. Therefore it should be emphasized that the curve for the overloaded cell (Figure 19) is above that of the normal cell because P_R has been affected more drastically than P_K. More specifically, for the blocked-orifice determinations, the recoil pressure appears to be abnormally low, especially at lower temperatures. Furthermore, there appears to be an exponential dependence of the _increase_ of P_R (the decrease in P_K/P_R) with increasing temperature. The particular condensed phase present has no apparent influence on the results.

The significance, if any, of these results is as yet unexplained. The possibility exists that, because of the abnormal manner of vaporization, species more complex than CaF_2 are affecting the value of P_R, but no other evidence is available to support this possibility. If such were the case, however, the temperature trend in Figure (19) would be interpreted as an exponental decrease in the more complex species with increase of the temperature.

Toroidal Nuggets. The sample substances exhibited a surprising tendency to form molten toroids about the inner rim of the cell orifice (see Figure 11). On cooling, the toroids maintained an inner diameter which was the same as the diameter of the orifice rim. This means that the sample creeped up the slope of the orifice until it reached the orifice rim. Such toroids were produced with CaF_2 and Ag, and evidence of a collapsed toroid was observed for Au. All of the sample was involved in the formation of the toroid in each case. At no time was there any reason to believe the advance of the toroid had passed the inner rim, and, consequently, no reason to think the normal rate of effusion was

TABLE IV

CALCIUM FLUORIDE BLOCKED-ORIFICE DATA

Run	T, ^{o}K	P_K, dyne/cm^2	P_R, dyne/cm^2
17	1554	15.1	6.32
18	1683	61.3	31.6
19	1629	28.3	15.9
20	1611	43.3	29.1
21	1647	51.0	35.6
22	1638	43.0	27.0
23	1680	85.0	73.2
24	1626	39.0	23.4
25	1667	67.0	47.5
26	1620	49.3	40.7
27	1679	81.2	59.1
28	1614	30.3	19.5
29	1662	74.6	59.4
30	1639	41.3	28.7

32	1644	40.7	33.7
33	1644	46.9	34.5
34	1574	10.6	6.13

altered.[†]

Permeation of Graphite Walls by Gold and Silver Vapors. Other workers[16] have noted that silver vapor and perhaps tin vapor[30] permeate some types of graphite.

The present experimental system is ideally suited for measuring such permeation. Closed[22] Miker cells were constructed to be identical to the normal cell (Figure 11) except that the orifice is replaced by a flat, closed bottom.

The rate of permeation of Ag and Au vapors through the walls of the closed cell was measured and appears in Table V. At a given temperature the rate of permeation for both silver and gold is (on the average) about 3% of their normal effusion rate at that temperature. The fact that permeation does occur, however, implies that "normal" effusion contains a contribution from permeation. Edwards and Downing[16] have studied this phenomenon and have demonstrated that at least two mechanisms exist by which metal vapors can permeate graphite walls. The vapors may undergo capillary effusion which obeys the Knudsen equation (except that the orifice area is ambiguous), or, activated diffusion may occur (Jost[35], Barrer[2]). The simplest method for distinguishing the above mechanisms appears to be that of performing a Knudsen-type calculation on the permeation data and comparing the results to effusion data; if a significant difference is observed in the slopes of log P_K vs. $1/T$ curves, for example, then the permeation is of a non-effusion

---

[†]An exception to this statement must be allowed for some runs made with Au in a cell of inferior design. Results indicating a blocked orifice were obtained, but on changing to a normal cell the results were in agreement with the statement above.

TABLE V

PREMEATION OF CLOSED GRAPHITE CELLS BY GOLD AND SILVER VAPORS

Gold		
Run	Temp., ^{O}K	μg/sec
1	1685	0.187
2	1653	0.105
3	1628	0.059
4	1590	0.006

Silver		
Run	Temp., ^{O}K	μg/sec
1	1393	0.413
2	1577	11.1
3	1476	2.50
4	1420	1.07
5	1367	0.470
6	1647	22.4

type. If the slopes agree, permeation results from capillary effusion with zero energy of activation.

The workers mentioned above concur that capillary-effusion obeys the Knudsen equation except that a simple parameter, usually assumed to be negligibly dependent on temperature appears in place of the orifice area. If this is true, then permeation data can be tested by applying the Knudsen equation directly, with an arbitrary constant for the parameter mentioned above. The P_K values calculated in this manner bear no necessary relation to any actual pressure, but the $\log P_K$ vs. $1/T$ plot will have the correct slope. To show this let a' be the unknown parameter for the Knudsen equation. Then from equation (1) and the above discussion, we have

$$a'P_K = \frac{w}{t}\sqrt{\frac{2\pi RT}{M}} \, , \tag{38}$$

from which the product $a'P_K$ can be calculated. Then if the data are effusion results, we expect a straight line for

$$\log(a'P_K) \text{ vs. } 1/T, \tag{39}$$

which implies

$$\log(a'P_K) = A/T + B, \tag{40}$$

or

$$\log P_K = A/T + (B - \log a'), \tag{41}$$

in which the original slope is retained.

Calculations were performed for the permeation data of Table V; for convenience a' was assigned numerical values: for the silver closed-cell data a' was assumed to be the area of the Miker cell used with silver; for the gold closed-cell data (Table II) a' is the area of the Miker cell used with gold. Results of these calculations appear as $\log P_K$ vs. $1/T$ plots in Figures (20) and (21).
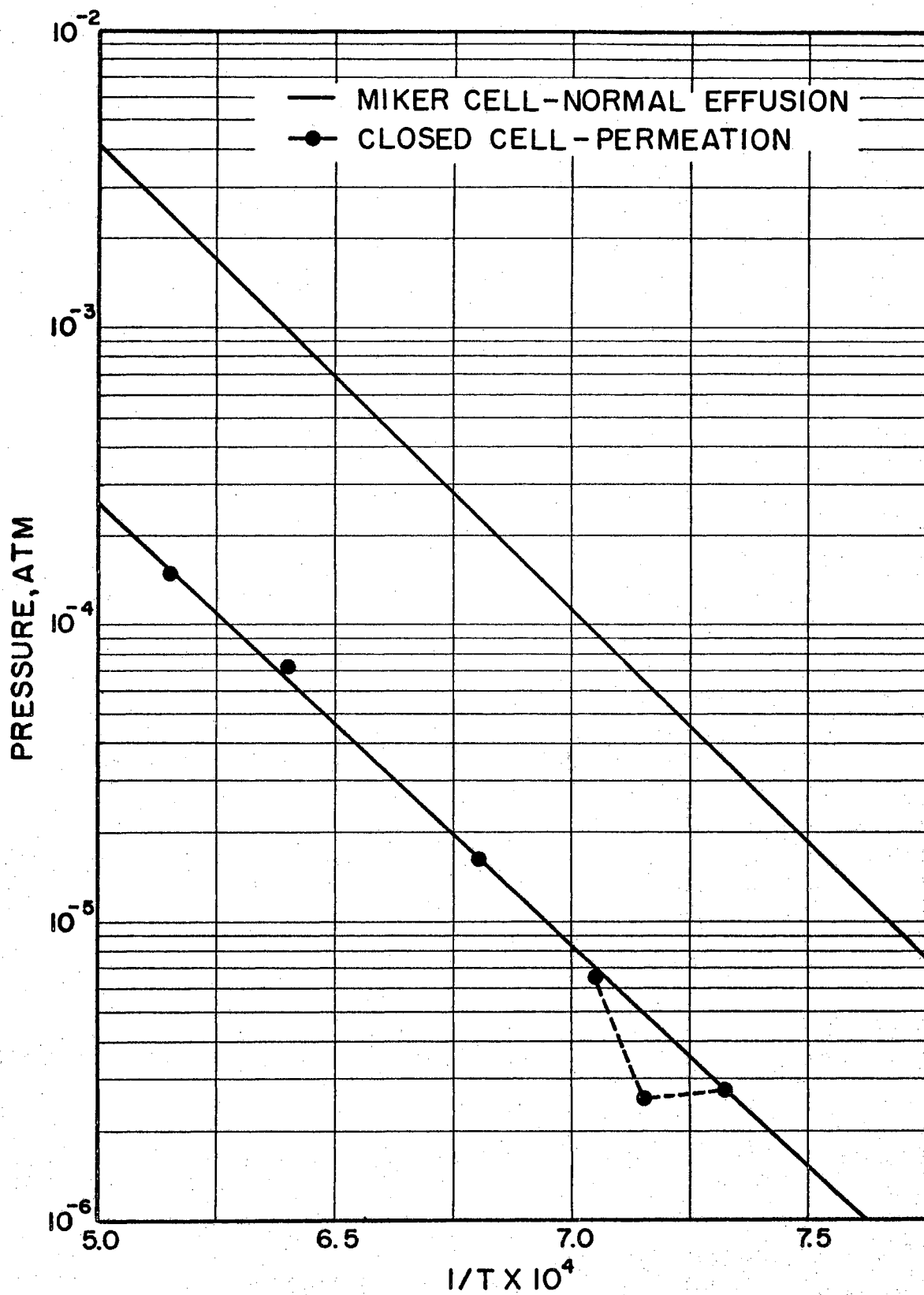
Figure 20. Normal Effusion and Closed-Cell Permeation, Silver.
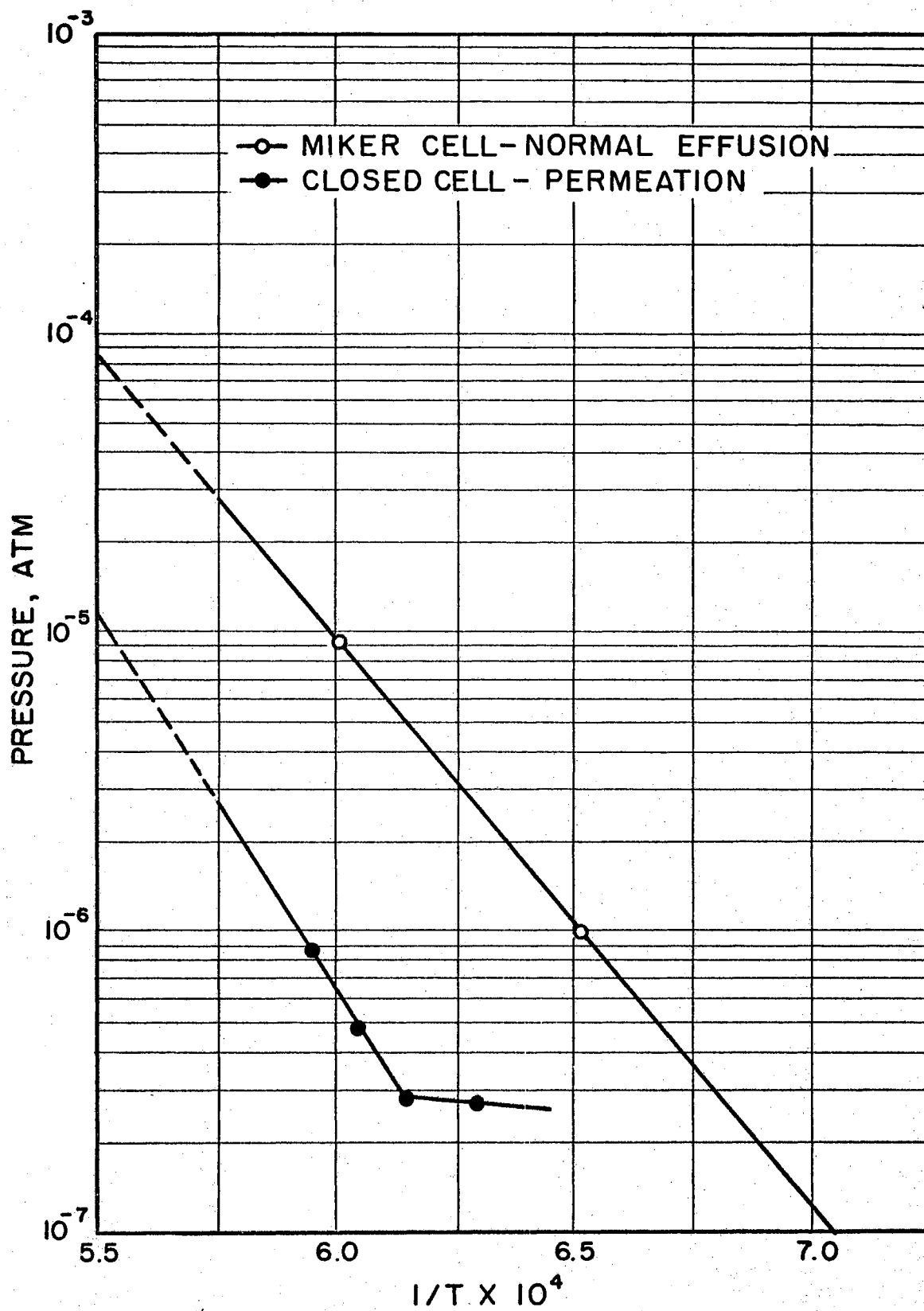
Figure 21. Normal Effusion and Closed-Cell Permeation, Gold.

The permeation data in Figure (20) yield a slope of -15900. The slope from the Miker cell data is -15000. The difference in slope of 900 is insufficient to confirm a permeation mechanism other than just effusion.[*] Edwards and Downing also studied silver permeation and they interpreted slope agreement within 700 to indicate no new mechanism.

The significance of the one anomalous point in Figure 20 is not understood. It is not attributed to scatter in the data because the magnitude of the error would be abnormal for typical Miker precision.

The possibility of a discontinuous change in mechanism exists. This is especially interesting because the same behavior appears for gold in Figure (21). The gold permeation data yield a slope of -24850, and the slope from the Miker data is -19964. The difference, nearly 5000, is interpreted as the appearance of a diffusion mechanism, rather than just capillary-effusion.

The slope given above corresponds to $A = \Delta H_{vap}/2.303R$ in equation (56), from which a ΔH_{vap} can be calculated for the diffusion-permeation and for the normal effusion. The difference between the ΔH_{vap} values thus calculated yields the energy of activation for the permeation by gold of the graphite cells used here. The resulting value, 22.5 Kcal/mole, is comparable to values usually found for the diffusion of gases through metals and solids[2, 35].

Edwards and Downing have pointed out that their results on copper permeation of graphite walls by activated diffusion imply that copper must be to some extent soluble in the graphite. The same comments

---

[*] However, strictly on the basis of the slope differences and the resulting ΔH_{vap} values, the heat of activation for diffusion of silver through the graphite wall is calculated to be 4.1 ± 0.88 kcal/mole.

appear applicable to the present work with gold, especially in light
of difficulties which the author has reported previously concerning
gold-graphite interaction[3].

An error is introduced in the above calculations by ignoring the
permeation contribution to "normal" effusion. Thus the quantity ω/t
which previously has been dealt with as pure rate of effusion could
possibly be the sum of three terms:

$$\omega/t = \dot{\omega} = \dot{\omega}_1 + \dot{\omega}_2 + \dot{\omega}_3, \tag{42}$$

where

$\dot{\omega}_1$ = pure effusion from orifice in time $\underline{t}$;

$\dot{\omega}_2$ = capillary effusion in time $\underline{t}$;

$\dot{\omega}_3$ = activated (capillary) diffusion in time $\underline{t}$;

and the generalized Knudsen equation becomes

$$P = (\sum_{i=1}^{3} \dot{\omega}_i)(2\pi RT/M)^{\frac{1}{2}}/a', \tag{43}$$

where $\underline{a}'$ is the appropriate area for each mode of weight loss. When
$\dot{\underline{\omega}}_1$ is sufficiently large that

$$\sum_{i=1}^{3} \dot{\omega}_i \approx \dot{\omega}_1, \tag{44}$$

obviously the error can be ignored. Such was considered to be the case
for the effusion data presented in the following sections.

Vapor Pressure and Molecular Weight Results. Two types of measure-
ments were performed. The first involved measurement of both the rate
of effusion and the recoil force. Results for silver, tin, and calcium
fluoride appear in Tables VI, VII, and VIII, respectively. The value
of the average molecular weight $\underline{M}^*$ of the effusing species is presented
as calculated directly from $\underline{P}_K$ and $\underline{P}_R$ without considering effusion

TABLE VI

VAPOR PRESSURE AND RECOIL FORCE DATA FOR SILVER

Run	T, °K	Rate of Effusion, μg/sec	Recoil Mass[†] m, mg	Pressure, dynes/cm^2 P_K	P_R	M^* uncorrected	M^* corrected[‡]
(Quartz Miker Cell)							
2	1323	2.29	0.0360	6.56	2.46	767	70
3	1327	2.19	0.0518	6.27	3.26	398	56
4	1323	2.26	0.0548	6.48	3.44	384	67
5	1322	1.78	0.0343	5.10	2.19	586	53
6	1316	1.75	0.0260	5.02	1.63	1020	70
7	1314	1.75	0.0332	5.02	2.08	628	62
8	1313	1.86	0.0433	5.32	2.72	404	59
9	1313	1.99	0.0490	5.68	3.06	372	61
10	1315	2.03	0.0475	5.81	2.98	412	64
11	1315	1.57	0.0288	4.50	1.81	670	58
						Average	62 ± 5
(Graphite Miker Cell)							
6	1333	5.42	0.150	32.7	19.9	292	62
7	1333	4.50	0.112	27.4	14.9	364	74
8	1333	5.40	0.116	32.8	15.5	484	81
9	1333	5.17	0.116	32.3	15.5	468	74
						Average	73 ± 5

[†]Recoil mass $\underline{m}$, is the mass which, under the acceleration of gravity, counterbalances the recoil force acting on the cell.

[‡]See Appendix A.

TABLE VII

VAPOR PRESSURE AND RECOIL FORCE DATA FOR TIN

Run	T, $^{\circ}$K	Rate of Effusion, μg/sec	Recoil Mass* m, mg	Pressure, dynes/cm^2 P_K	P_R	M* uncorrected	M* corrected
2	1504	5.03	0.191	12.2	9.41	197	64
3	1393	1.07	0.0365	2.49	1.80	226	83
4	1332	1.51	0.0613	3.54	3.08	157	100
6	1386	5.60	0.210	13.0	10.4	186	121
7	1434	6.26	0.239	14.9	11.8	189	106
8	1384	3.26	0.149	7.61	7.33	124	81
9	1408	2.88	0.123	6.75	6.10	141	85
10	1393	0.94	0.0367	2.18	1.83	172	69
11	1393	0.98	0.0318	2.28	1.65	226	85
12	1418	1.32	0.0448	3.10	2.21	234	76
13	1418	1.54	0.0497	3.62	2.44	261	86
14	1418	1.58	0.0511	3.72	2.52	259	88
15	1418	1.75	0.0600	4.12	2.96	230	77
16	1466	10.1	0.377	23.6	18.5	199	106
17	1466	9.90	0.350	23.6	18.2	200	112
18	1334	0.58	0.0211	1.32	1.04	192	94
19	1334	0.63	0.0202	1.44	0.995	249	114
20	1334	0.70	0.0238	1.60	1.17	223	108

Average 92 ± 14

*Recoil mass $\underline{m}$, is the mass which, under the acceleration of gravity, counterbalances the recoil force acting on the cell.

TABLE VIII

VAPOR PRESSURE AND RECOIL FORCE DATA FOR CALCIUM FLUORIDE

Run	T, ^{o}K	Rate of Effusion, μg/sec	Recoil Mass* m, mg	Pressure, dynes/cm^2 P_K	P_R	M^* uncorrected	M^* corrected
1	1605	4.07	0.241	31.8	31.9	78	71
3	1568	1.75	0.102	13.6	13.6	78	70
4	1577	2.00	0.111	15.5	14.8	86	79
8	1676	8.06	0.455	64.6	62.2	84	75
9	1646	6.27	0.327	49.8	43.5	103	91
10	1631	3.02	0.156	23.9	20.8	103	68
11	1682	9.95	0.528	79.9	69.8	102	86
12	1584	2.23	0.115	17.4	15.3	101	84
13	1581	1.86	0.090	14.4	11.9	114	90
14	1521	0.75	0.036	5.77	4.79	112	100
15	1650	3.63	0.184	28.9	24.3	110	62
16	1707	12.5	0.685	101.0	90.6	91	66
35	1579	1.40	0.0663	10.8	8.82	117	76
36	1571	1.08	0.0490	8.34	6.52	128	75
37	1570	1.07	0.0548	8.26	7.29	100	69
38	1611	2.76	0.132	21.4	17.6	115	81
39	1626	2.76	0.143	21.8	19.0	103	71
40	1610	2.44	0.118	19.2	15.7	117	77
41	1618	2.42	0.125	19.0	16.6	102	72
42	1619	2.42	0.114	19.0	15.1	124	76

Average 77 ± 7

*Recoil mass m, is the mass which, under the acceleration of gravity, counterbalances the recoil force acting on the cell.

during the cooling step, and also in the corrected form according to Appendix A.

The second type of determination involved measurement of just the rate of effusion, and therefore of P_K only. Results appear in Tables IX, X, and XI for silver, calcium fluoride, and gold, respectively. Figures 22, 23, and 24 present conventional log P_K vs. 1/T for these same substances. The data for gold, Table XI and Figure 24, were obtained with Control System II.

For the data involving measurement of just the pressure P_K, the Knudsen equation was applied directly. Correction factors $\underline{W}$ and $\underline{F}$ were obtained by interpolation from Table I. In all cases the monomeric value for the molecular weight $\underline{M}$ was used to calculate P_K.

TABLE IX

VAPOR PRESSURE OF SILVER FROM RATE OF EFFUSION

Run	Temp., $^\circ$K	Rate of Effusion, μg/sec	Pressure, $P_K/10^{-6}$atm
10	1378	9.62	58.7
11	1325	2.94	17.6
12	1293	1.94	11.5
13	1228	0.301	1.74
14	1458	32.5	203.
15	1298	16.4	9.15
16	1345	5.15	31.0
17	1255	0.953	5.55
18	1395	10.9	68.0
19	1248	0.558	3.26
20	1223	0.348	2.00
21	1185	0.157	0.892
22	1150	0.051	0.284
23	1350	4.22	25.0
24	1323	2.52	15.2
25	1290	1.47	8.70
26	1240	0.511	2.97
27	1200	0.207	1.18

TABLE X

VAPOR PRESSURE OF CALCIUM FLUORIDE FROM RATE OF EFFUSION

Run	Temp., $^{\circ}K$	Rate of Effusion, $\mu g/sec$	Pressure $P_K/10^{-6}$ atm
1	1668	9.20	74.6
2	1648	5.92	46.7
3	1600	3.26	25.2
4	1568	1.73	13.3
5	1535	1.07	8.12
6	1520	0.68	5.04
7	1503	0.45	3.38
8	1488	0.25	1.88
9	1463	0.18	1.34

TABLE XI

VAPOR PRESSURE OF GOLD FROM RATE OF EFFUSION

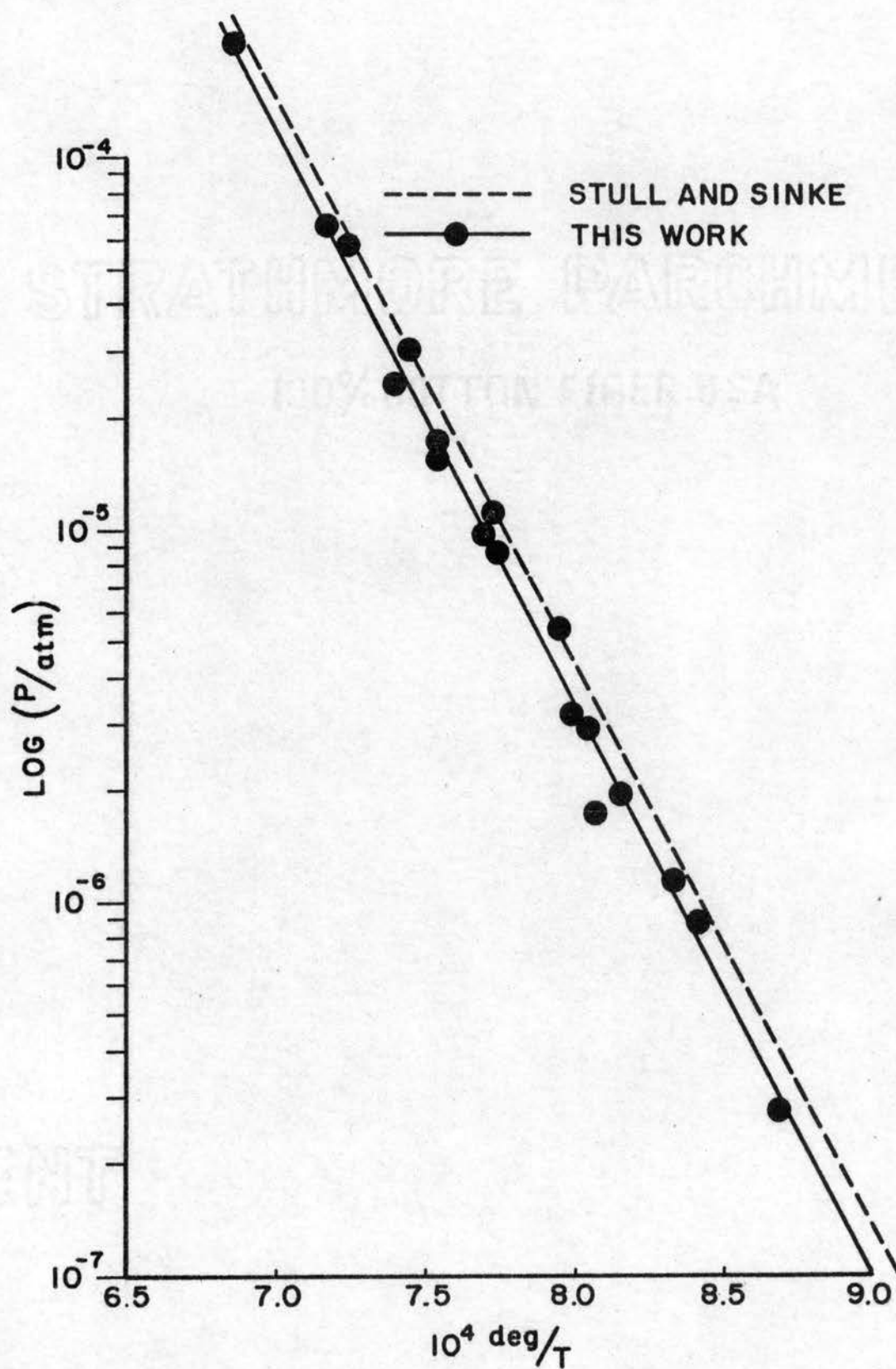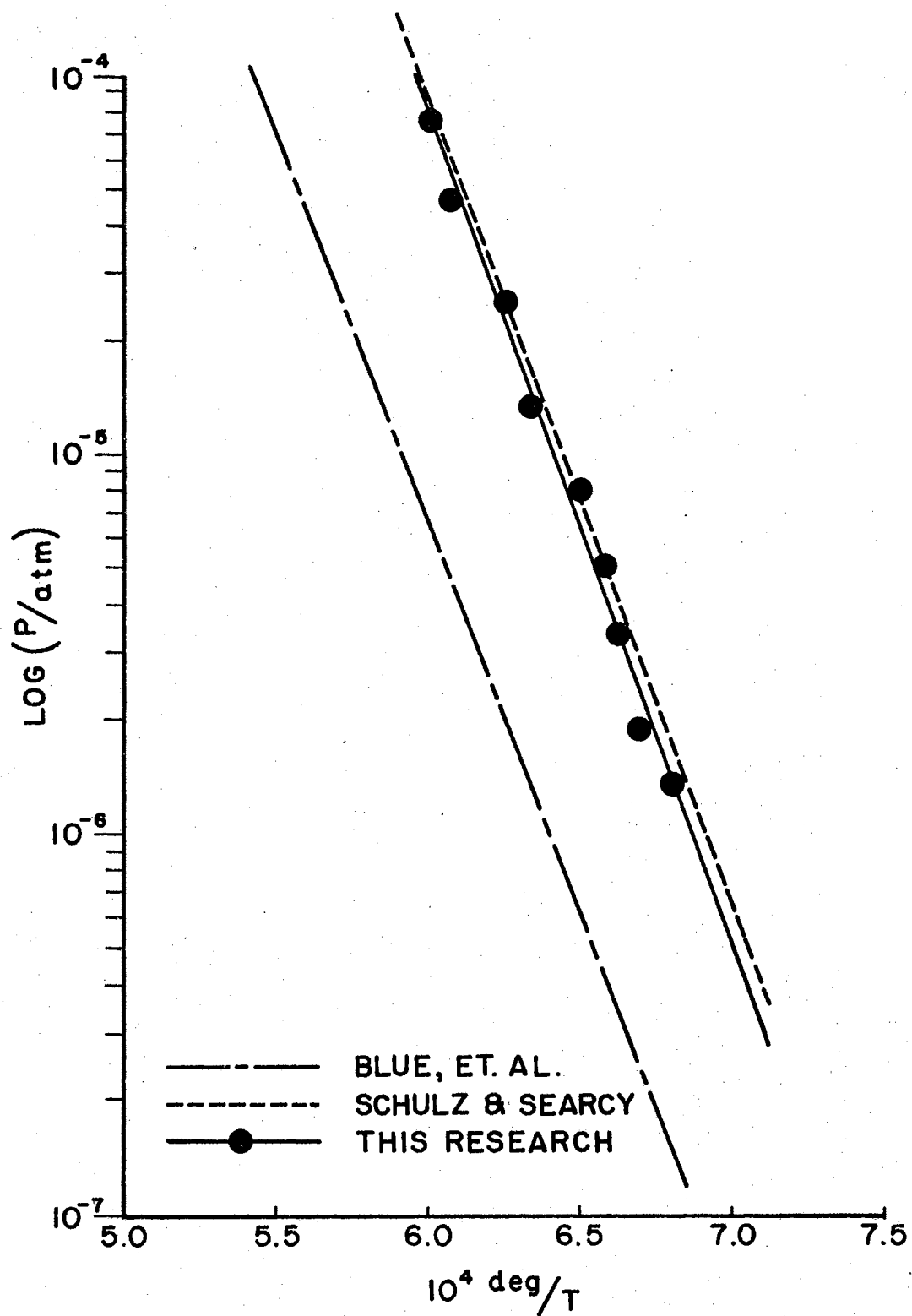| Run	Temp., $^{\circ}K$	Rate of Effusion, $\mu g/sec$	Pressure $P_K/10^{-6}atm$
26	1673	3.72	12.5
27	1652	2.82	9.44
28	1625	1.72	5.68
29	1597	1.07	3.50
30	1585	0.89	2.91
31	1569	0.70	2.30
32	1563	0.56	1.83
33	1548	0.42	1.36
34	1533	0.32	0.98

Figure 22. Vapor Pressure of Silver.

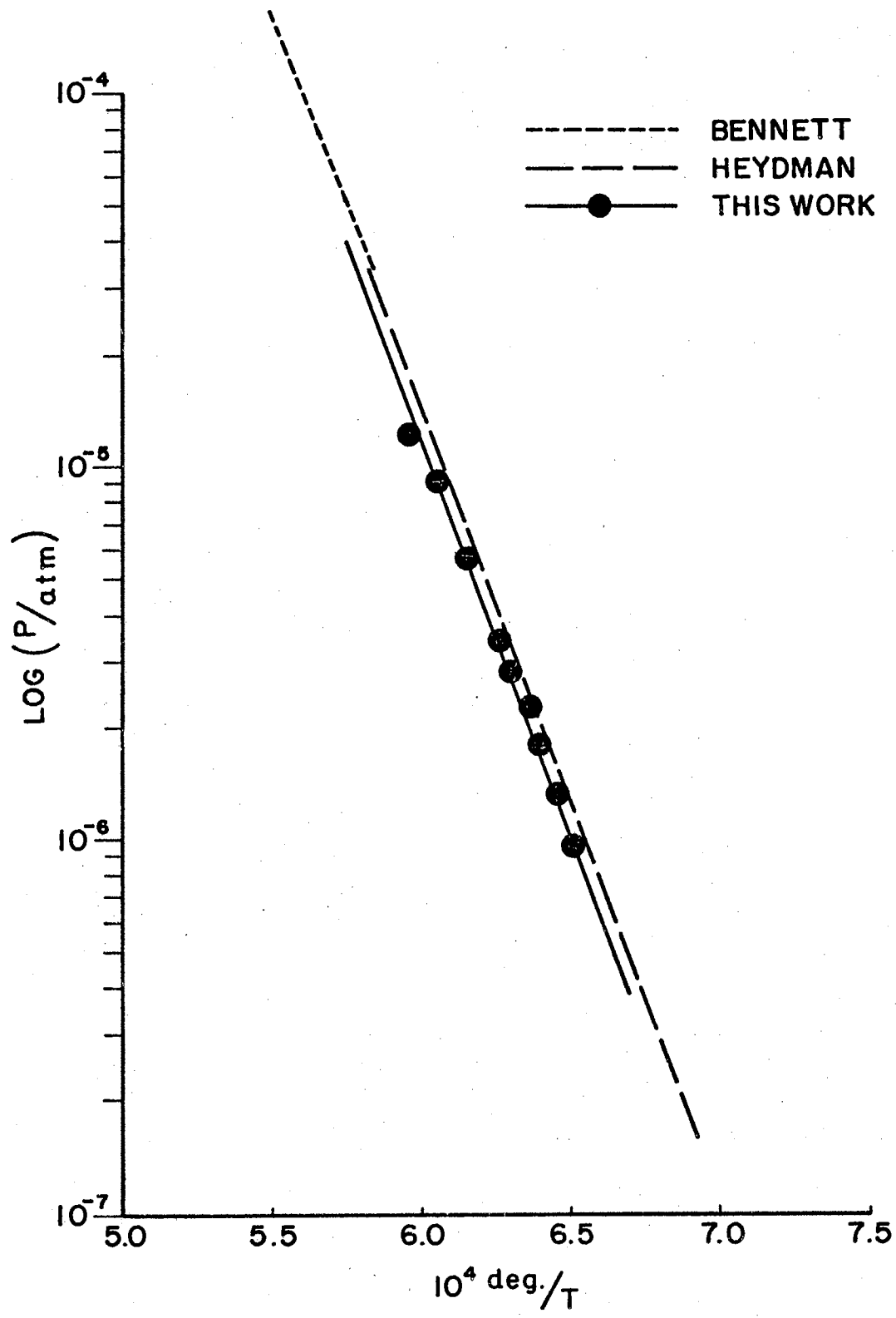Figure 23. Vapor Pressure of Calcium Fluoride.

Figure 24. Vapor Pressure of Gold.

CHAPTER V

INTERPRETATION OF RESULTS

Discussion. The particular sample substances employed were chosen

not so much because of any particular interest in their vapor pressures

and thermodynamic properties (though these are valuable data), but

rather to provide presumably well-behaved systems for testing the Miker

technique. Each sample substance is easily obtained, inert towards

graphite, and sufficiently well studied by earlier workers so that

considerable data are available for purposes of comparison.[*]

The internal consistancy of the Miker technique is demonstrated

by the experimental results in the last chapter, and, though the average

molecular weight values are not of the precision which was sought

initially, they are considered sufficiently reliable to distinguish

between vapors which differ in complexity by integral values, i.e., Ag,

Ag_2, etc.

Once the matter of internal consistancy is accepted, even though

problems with the technique still exist,[**] the data can be compared

in a meaningful manner with results of other workers. This is the

purpose of the following sections.

Silver. Average values for the molecular weight of silver using

_____

[*]Calcium fluoride is not as well studied as the others.

[**]See the section on Suggestions for Further Work.

quartz and graphite Miker cells are 42.5% and 32.5% low, respectively

(based on a molecular weight of 108). These are clearly impossible

results, but nevertheless encouraging because the mean deviation is only

± 5 which suggests the presence of a systematic discrepancy. It is

possible that the P_K pressures should be higher, which would cause the

ratio $(P_K/P_R)^2$, and therefore the uncorrected molecular weight $\underline{M}^*$, to

be larger. Correction of $\underline{M}^*$ for effusion while cooling would then

result in generally larger molecular weight values. This is not con-

sidered a likely possibility, however, because the P_K values are already

slightly larger than they should be as the result of ignoring the

permeation known to occur. Furthermore, as will be shown shortly,

the P_K values are in good agreement with data from other sources.

Another possibility, considered more likely, is that the cor-

rected molecular weights are overcorrected (Appendix A). In effect,

the correction for effusion during cooling, if in error by 20% for

example, would decrease (for a negative error) the corrected value of

P_R by 20%, and the corrected value of $\underline{M}^*$ by 40% because of the second

power relation between these two quantities. The source considered

most likely for such an error is the experimental cooling law obeyed

by the Miker cell, about which some question has already been raised.

It appears quite reasonable to say that the values 62 ± 5 and

73 ± 5 obtained in this work must be interpreted as fixing the most

predominant species in silver vapor as the monomer. The strongest

support for this interpretation has not been mentioned. The average

molecular weight values for CaF_2 and Sn are unquestionably those of

the monomeric species. Furthermore, the findings of other workers (to

be discussed) support these results. If the results for CaF_2 and Sn

are accepted and compared to those for Ag, the monomeric value of the molecular weight follows.

Considerable confusion exists in the literature on the molecular weight of silver vapors. Freeman[18] has discussed this matter more thoroughly. First the Stern-Gerlach experiment[57], which demonstrated the quantization of the atomic magnetic moment, is successful for silver vapor, a result which depends on monatomic species. But Nernst[47] reported molecular weights of 352 at 1885°, 351 at 1945°, 214 at 1990°, and 174 at 2035° from the Victor Meyer method[64]. A value of 127 ± 20 was reported by von Wartenburg[61] using the same method. Searcy and Freeman[53] reported 260 ± 90 from their torsion effusion method, and furthermore, their findings were confirmed by Michel[46] with a mass spectrometric determination. The source of error, if any, has not been established for these various results. Those of Searcy and Freeman stand out particulary in this regard, for they not only excerised careful technique with the torsion-effusion method, but also obtained, concurrent with the silver data, results for germanium and tin which are quite reasonable.

The vapor pressure data for silver in Table IX are in good agreement with those of other workers, as shown in Figure 22. A least squares solution of the data in Table IX, yields log P ± 6.5781 – 15001/T. The heat of sublimation of silver at 298°K, calculated from the P_K data in Table IX, appears in Table XII. Free energy functions for the calculation are from Stull and Sinke[59]. The average value for the heat of sublimation of silver at 298°K is 68.50 ± 0.44 kcal, which agrees quite well with 69.1 calculated by Kelley[37] from Harteck's data[27], with 67.8 ± 0.6 kcal obtained by Schadel and Birchinall[51], and 69.0 ± 0.5 kcal by Searcy and Freeman[53].

TABLE XII

HEAT OF SUBLIMATION OF SILVER FROM RATE OF EFFUSION DATA

$T^O K$	$\Delta F^O/T$	$-fef(g)$	$-fef(1)$	$\Delta H^O_{298}/T$	ΔH^O_{298}
1378	19.36	45.05	15.27	49.14	67715
1325	21.75	44.90	14.96	51.70	68502
1293	22.60	44.81	14.80	52.61	68025
1228	26.35	44.60	14.46	56.49	69370
1458	16.89	45.23	15.66	56.50	67797
1298	22.92	44.82	14.83	52.92	68690
1345	20.73	44.95	15.07	50.51	67936
1255	24.04	44.68	14.59	54.14	67946
1395	19.06	45.08	15.35	48.80	68076
1248	25.10	44.66	14.56	55.21	68902
1223	26.07	44.59	14.43	56.24	68782
1185	27.68	44.46	14.26	57.88	68588
1150	29.95	44.35	14.08	60.23	69264
1350	21.05	44.96	15.10	50.92	68742
1323	22.04	44.90	14.96	51.99	68783
1290	23.15	44.79	14.91	53.04	68422
1240	25.29	44.63	14.51	55.42	68721
1200	27.12	44.51	14.30	57.33	<u>68796</u>

Average 68503 ± 441

$-fef(g) = [-(F^O - H^O_{298})/T]g$

$-fef(1) = [-(F^O - H^O_{298})/T]1$

<u>Tin</u>. The average value of $\underline{M}^*$ from Table VII is 92 ± 14 which is low (based on 119), but in good agreement with a mass spectrometric determination by Honig and the 91 ± 29 obtained by Searcy and Freeman[53]. Results which suggest the vapor species to be Sn_4 were obtained by von Wartenberg[61] with a static method. The possibility of the vapor being Sn_4 must, however, be rejected in view of the above results.

Considerable scatter among vapor pressure determinations was obtained for Sn. This was the result of difficulty experienced concurrently with the shutter mechanism which shields the optical system from the Miker cell and ordinarily prevents the accumulation of a metallic deposit which would cause erroneous temperature measurements. Because the P_K data for Sn are less reliable than they would have been, had this shielding difficulty not occurred, no heat of sublimation values are presented. It should be emphasized that, though the vapor pressure data are considered unacceptable for calculating the heat of sublimation, they are quite acceptable for molecular weight determinations. This is because the factor $(P_K/P_R)^2$, which determines the effect of error on the molecular weight, is effected by less than 10% even if the temperature were incorrect by 100 deg.

<u>Calcium Fluoride</u>. The molecular weight of CaF_2 vapor has not been determined directly previous to this work. Hammer[26] found magnesium fluoride to vaporize as monomers. The only gaseous calcium fluoride yet observed spectroscopically is $CaF_{(g)}$, but Shulz and Searcy[52] have noted that the total pressure to be expected from the reaction $CaF_{2(1)} \rightleftharpoons CaF_{(g)} + F_{(g)}$ would be several orders of magnitude below observed vapor pressures. They also note that dissociation to elemental calcium and fluorine gas is negligible, and conclude that CaF_2 vaporizes primarily

to monomer molecules.

The molecular weight value 77 ± 7 obtained in this work (Table VIII) agrees with the comments above, i.e., that the predominant vapor species is CaF_2.

The P_K values in Table X are in good agreement with the torsion pressures of Shultz and Searcy as shown by Figure 23. A least squares solution of the data in Table X yields log P_K = 8.4016 - 20872/T.

Gold. Only P_K determinations were made for Au because at the time gold was studied, the primary interest was the conversion of the balance control system from the original one requiring the telemicroscope to the C.A.T. controller employing the Photopot null sensor and remote control.

The P_K data from Table XI are plotted as log P_K vs. 1/T in Figure 24. A least squares solution of the effusion data in Table XI yields log P_K = 7.0184 - 19964/T.

The heat of sublimation of gold at 298°K, calculated from the third law method, appears in Table XIII. The value 88.13 ± 0.21 kcal is based on gold vapor being monomeric. The expressed uncertainty is the mean deviation. The value 88.13 ± 0.21 kcal agrees well with the value 86.7 ± 0.5 kcal obtained by this author in an independent experimental system[3], and also with the value 88.4 kcal obtained by Heydman[28] in this laboratory with the conventional Knudsen method. Other values for this quantity are 90.5 by Kelley[37], 84.7 by Stull and Sinke[59], and 86.5 by Hildenbrand[30].

Evaluation of the Miker Technique. There are several advantages:

1. Rate of effusion and recoil force are determined essentially simultaneously with the same detector, i.e., the microbalance.

TABLE XIII

HEAT OF SUBLIMATION OF GOLD FROM RATE OF EFFUSION DATA

$T^{O}K$	$\Delta F^{O}/T$	$-fef(g)$	$-fef(1)$	$\Delta H^{O}_{298}/T$	ΔH^{O}_{298}
1673	22.43	47.62	17.57	52.48	87800
1652	22.99	47.56	17.46	53.09	87700
1625	24.00	47.50	17.35	54.15	88010
1597	24.96	47.42	17.23	55.15	88060
1585	25.33	47.39	17.17	55.55	88040
1569	25.79	47.35	14.10	56.06	87960
1563	26.25	47.34	17.08	56.51	88350
1548	26.84	47.30	17.01	57.13	88440
1533	27.59	47.25	16.91	57.93	88810

Average 88130 ± 271

$$-fef(g) = [-(F^{O} - H^{O}_{298})/T]g$$

$$-fef(1) = [-(F^{O} - H^{O}_{298})/T]1$$

2.   A single Miker run consists of a series of null determinations
(manual balance control) or a constant null determination (auto-
matic balance control), either of which provides continuous con-
firmation of the rate of effusion. A Knudsen determination with
a conventional cell, on the other hand, employs only the initial
and final weight of the cell to determine the rate of effusion,
and any deviation from this "average" rate of effusion during
the run is never detected.

3.   Errors in balance calibration and orifice area measurement
cancel in the calculation of molecular weight of the vapor since
it is the _ratio_ of rate of effusion to recoil force which is
required.

4.   Measurements of rate of effusion and of recoil force can be
made rapidly and over a wide temperature range without intermittent
opening of the vacuum system. Thus, for example, the calcium
fluoride P_K determinations (Figure 23) required less than two
hours of operating time, a feat which might very well require two
days of rather hard work to accomplish by conventional Knudsen
technique.

5.   The Miker cell serves as an excellent black body for pyrometric
determinations of temperature.

6.   The orifice is located "within the cell," which should minimize
cold orifice problems.

7.   Effusion downward, away from the microbalance, minimizes dif-
ficulties with condensation on suspension wires.

8.   Temperature gradients should be minimized by the cylindrical
symmetry of the Miker cell, coupled with the cylindrical resistance

heating element.

The apparent disadvantages of the technique are:

1. The recoil force measurement is quite sensitive to the mass which effuses during the cooling period of a run, and the necessarily large correction is objectionable.

2. The transmission probability W and force factor f are strictly theoretical quantities; these factors require experimental confirmation before they can be used with complete confidence.

The accuracy of the molecular weight values reported in the last chapter are comparable to those reported by other recoil techniques. However, they are not good enough to establish the technique as outstandingly useful for such purposes. This is considered a direct measure of the stage of development of the technique and does not indicate any inherent limitation or experimental barrier. Suggestions for increasing the accuracy of the recoil measurements appear in the next section.

The rate of effusion data are unsurpassed among methods for making such measurements at high temperatures. Torsion-effusion techniques match the sensitivity of the VMB-1, but as has already been mentioned, each determination of the slope of the rate of effusion curve employs only the initial and final weight of the torsion-cell. This entails end corrections for effusion that occurs while heating to and cooling from the temperature of the run. Suspending the torsion cell from a microbalance is an obvious solution to this problem, and has been tried, but the practicality of this innovation is doubtful because two detectors must be calibrated, i.e., the torsion suspension and the microbalance.

The Langmuir-recoil technique developed by Bader[1] requires pyrometric sightings onto an open surface rather than into a blackbody orifice as

for a Miker (or torsion) cell, and thus necessitates emissivity correc-
tions which are undesirable. The effusion which occurs during cooling
interferes with the recoil force measurement just as for the Miker tech-
nique, though Bader's sample arrangement should cool more rapidly than
the Miker cell. Apparently this effect was overlooked by Bader. The
relatively large sample area (approximately 1 cm^2) employed by Bader
results in a recoil force larger than that from a Miker cell. It is
doubtful if the system employed by Bader could be used to study vapors
above liquid condensed phases. First, containing the liquid on the
small tungsten pan (Chapter I) would probably be difficult and, second,
the surface area of the liquid phase, a necessary parameter in equation
(2), would be inaccessible.

Suggestions for Future Work. Future work with the Miker technique
falls naturally into two areas: (1) further development of the technique
itself; (2) application of the technique to systems other than those
reported here.

Further development of the Miker technique should involve the fol-
lowing:

1. The automatic control system must be put into operation.
Reasons for desiring automatic control have been presented and
will not be restated here. It will be emphasized, however, that
there is every reason to believe that Control System II, described
in Chapter III, will provide the desired control, and all that
remains is the testing of various control parameters in order to
match them with the control requirements. In any case, the problem
of automatically controlling a microbalance has been solved success-
fully by other workers, and is not regarded as a permanent limitation

to the technique.

2.   The problem of effusion which occurs during cooling is quite
serious because, even with accurate rate of cooling data, the
magnitude of the corrections involved is objectionably large.
The solution of this problem apparently will require a new furnace
design, i.e., one which inherently cools much faster than the one
employed in this work. Electron bombardment heating[3] and thin-
element resistance heating appear attractive for this purpose.
Radiofrequency induction heating appears questionable, because of
the possibility of spurious inductive forces on the Miker cell.
To further increase the rate of cooling, Miker cells should be
designed to possess minimum heat capacity. Very thin metal cells
are therefore recommended when sample-cell interaction permits
their use. The possibility of constructing a thin metal cell and
then coating it with an ultrathin layer of some inert substance,
e.g., BN, has been proposed[19].

Application of the Miker technique to high temperature studies
represents a truly inexhaustible area for research. For example Margrave[44]
has pointed out: "Hundreds of diatomic molecules remain to be discovered."
The number of more complex molecules yet to be discovered in the vapor
phase is probably inestimable, and even for known vapor species, reliable
thermodynamic data is meager (Chapter I).

Besides the rate of effusion and recoil data which the Miker tech-
nique provides, other types of study are suggested. Direct combination
of the Miker and mass spectrometric techniques is proposed. Porter[49]
has already shown how such a combination, but with conventional Knudsen
effusion, offers a means of determining accommodation coefficients for

gaseous species in evaporation processes of the type nX(condensed) = $X_n(g)$. Such a combination with the Miker technique should not only be more convenient, but also simplify the analysis of the mass spectrometric data. Furthermore, the Miker technique effusion data leads to more accurate heats of sublimation than mass spectrometric data, if the identity of the various vapor species can be determined, and the latter is best accomplished mass spectrometrically.

The Miker technique might possibly be employed to test the validity of the correction factors f and W. For example, if a given substance were studied with a range of Miker cells of various orifice dimensions, but always under conditions such that one would predict $P_{K1} = P_{K2} = ...P_{KN}$, and therefore $P_{R1} = P_{R2} = ...P_{RN}$, where the Nth subscript, for example, identifies the Nth Miker cell, then from equation (21) one can derive

$$m_1/f_1 = m_2/f_2 = ...m_N/f_N .$$
(45)

Rearrangement of (45) yields, for example,

$$m_1/m_2 = f_1/f_2,$$
(41)

which predicts that the ratio of the measured recoil masses m_1/m_2 when plotted against the ratio of the theoretically derived force factors will always yield a straight line with slope equal to unity. The same type of test is available for the relation between experimental effusion data and derived transmission probabilities. A "multicell" experiment of this type has been developed in this laboratory using conventional Knudsen technique for testing the validity of transmission probabilities, and Freeman and Edwards[20] have described an experiment which proposes detailed examination of the molecular beam produced from any type of effusion cell orifice, and thus to test both f and W. The Miker technique

could aid these studies and, for that reason, has been associated with them.

The author would particularly like to see the blocked-orifice studies extended to determine the significance, if any, of the abnormal decrease of the recoil pressure with increase of temperature. This experiment would have to be performed with various sample substances to test the generality of the results obtained in this work with calcium fluoride.

The permeation studies should be extended over a wider range of temperatures, sample substances, and kinds of graphite (and other container materials).

The most obvious suggestion for future work with the Miker technique concerns the upper pressure limit of applicability of equations (1) and (20). The work of Schulz and Searcy[52] with calcium fluoride represents the only detailed investigation yet made of the high pressure limit to the force-of-effusion equation (torsion-effusion, equation (4)). Carlson[12] has investigated the high pressure limit to the Knudsen effusion equation (1). The Miker technique offers an extremely convenient way to study the "high-pressure limit" of molecular flow conditions for both recoil force measurements and total flow measurements. With an appropriate sample in the cell one could determine rapidly whether a given system would yield consistent data in the known molecular flow region; by simply increasing the temperature of the furnace, one could make the necessary measurements at higher and higher cell pressures; it would be possible to return at any time to lower temperatures and pressures to recheck the initial data.

As a final suggestion, the use of the Miker technique for the study

of non-equilibrium pressures is proposed. The determination of $\underline{M}^*$ does not require equilibrium values for $\underline{P}_K$ and $\underline{P}_R$, and actually, so long as mass effuses, the pressure inside the cell is less than the equilibrium pressure. If the vaporization coefficient is less than unity the steady-state pressure is lowered further. These effects are usually minimized by the use of vanishingly small orifices, but more study would be useful in the field.

SELECTED REFERENCES

1. Bader, M., Ph.D. Thesis, Indiana University (1961).

2. Barrer, R. M., "Diffusion in and Through Solids," Cambridge University Press, Cambridge, England (1941).

3. Bennett, J. E., M.S. Thesis, Oklahoma State University (1962).

4. Berkowitz, J. and Chupka, W. A., J. Chem. Phys. 29, 653 (1958).

5. Blakelock, H. D., and Machin, C. F., Engineer 196, 83 (1953).

6. Blue, G. D., et. al., J. Phys. Chem. 67, 877 (1963).

7. Bradt, Mohler, and Dibeler, J. Res. N.B.S. 57, 223 (1956).

8. Brewer, L. and Searcy, A. W., J. Am. Chem. Soc. 73, 5308 (1951).

9. Brewer, L. and Kane, J. S., J. Phys. Chem. 59, 105 (1955).

10. Brewer, L. and Searcy, A. W., Ann. Rev. Phys. Chem., 7, 259 (1956).

11. Cahn, L. and Shultz, H. R., in "Vacuum Microbalance Techniques," Vol. 2 (R. F. Walker, ed.) Plenum Press, New York (1962).

12. Carlson, K. D., "The Molecular and Viscous Effusion of Saturated Vapors," ANL-6156, Argonne National Laboratory, Argonne, Illinois (1960); also Ph.D. Thesis, University of Kansas (1960).

13. Chupka, W. A. and Inghram, M. G., J. Chem. Phys. 21, 371, 1313 (1953).

14. Cochran, C. N., in "Vacuum Microbalance Techniques," Vol. 1, (M. J. Katz, ed.) Plenum Press, New York (1961).

15. Drowart, J. and Honig, R. E., J. Phys. Chem. 61, 980 (1957).

16. Edwards, R. K. and Downing, J. H., J. Phys. Chem. 59, 1079 (1955).

17. Farber, M. and Darnell, A. J., J. Chem. Phys. 25, 526 (1956).

18. Freeman, R. D., Ph.D. Thesis, Purdue University (1954).

19. Freeman, R. D., Private Communication.

20. Freeman, R. D. and Edwards, J. G., To be published, J. Chem. Phys.

21. Gerritsen, A. N. and Damon, D. H., Rev. Sci. Instr. 33, 301 (1962).

22. Gilles, Cater and Plante, J. Chem. Phys. 32, 1269 (1960).

23. Goldfinger, Ackerman and Jeunehomme, Tech. Report AF 61(052)-19, Univ. of Brussels, Jan. 1959.

24. Gulbransen, E. A., in "Surface Studies with the Vacuum Microbalance: High Temperature Reactions," Advances in Catalysis, Vol. V (W. G. Frankenburg, et. al., ed.) Academic Press, New York, 1953, pp. 119-175.

25. Gulbransen, E. A. and Andrew, K. F., Vacuum Microbalance Techinques, Vol. 2 (R. F. Walker, ed.), Plenum Press, New York (1962).

26. Hammer, R. R., Ph.D. Thesis, University of California (1961).

27. Harteck, P., Z. physik. Chem. 134, 1 (1928).

28. Heydman, W. F., M.S. Thesis, Oklahoma State University (1959).

29. Hildenbrand, D. L., Aeronutronic Reports No. U-1988, U-2403, U-2231, U-2352, U-2116, Contract AF 04(611)-8523, 1963.

30. Hildenbrand, D. L., Private Communication.

31. Hodgman, C. D., "Handbook of Chemistry and Physics," Chemical Rubber Publishing Co., Cleveland, Ohio, 37th ed., 1955.

32. Honig, J. M. and Czanderna, A. W., Anal. Chem. 29, 1206 (1957).

33. Inghram, Chupka, and Porter, J. Chem. Phys. 23, 2159 (1955).

34. Inghram, M. G. and Drowart, J., in "Proceeding of an International Symposium on High Temperature Technology," McGraw-Hill Book Company, New York (1960).

35. Jost, W., "Diffusion in Solids, Liquids, Gases," Academic Press, New York (1952).

36. Kanes, J. S. and Reynolds, J. H., J. Chem. Phys. 25, 342 (1956).

37. Kelley, K. K., U. S. Bur. Mines Bull. 383, 1935.

38. Kennard, E. H., "Kinetic Theory of Gases," 1st ed., McGraw-Hill Book Co., New York (1938), pp. 6-9, 30, 60-71.

39. Knudsen, M., Ann. d. Physik. 6, 129 (1930).

40. Knudsen, M., Ann. d. Physik. 31, 205 (1910).

41. Knudsen, M., Ann. d. Physik. 31, 633 (1910).

42. Langmuir, I., Phys. Rev. 2, 329 (1913).

43. Margenau, H. and Murphy, G. M., "Mathematics of Chemistry and Physics," 2nd ed., D. van Hostrand Co., New York (1956).

44. Margrave, J. L., in "Proceeding of a Symposium on High Temperature - A Tool for the Future," Stanford Research Institute, Menlo Park, California (1956).

45. Meschi, D. J. and Searcy, A. W., J. Phys. Chem. 63, 1175 (1959).

46. Michel, M. C., Private Communication to A. W. Searcy.

47. Hernst, W., Z. Elektrochem. 9, 622 (1903).

48. Pearson, E. B., "Technology of Instrumentation," The English Universities Press Ltd., London (1957).

49. Porter. R. F. and Schoonmaker, R. C., J. Chem. Phys. 29, 1070 (1958).

50. Sandstede, G. and Robens, E., Chemie-Ingenieur Technik. 32, 6, 413 (1960); Translated in "Technical Bulletin No. 12," Brinkman Instruments, Inc., Great Neck, N. Y.

51. Schadel, W. M. and Birchinall, C. E., J. Metals 188, 1134 (1950).

52. Schulz, D. A. and Searcy, A. W., J. Phys. Chem. 67, 103 (1963).

53. Searcy, A. W. and Freeman, R. D., J. Am. Chem. Soc. 76, 5229 (1954); J. Chem. Phys. 23, 88 (1955).

54. Sheer, M. D., J. Phys. Chem. 61, 1184 (1957).

55. Shuttleworth, R., Rev. Sci. Instr. 32, 1327 (1961).

56. Simons, Shierrer and Ritter, Rev. Sci. Instr. 24, 36 (1953).

57. Stern, O. and Gerlach, W., Z. Physik. 8, 110 (1921); ibid 9, 349, 353 (1922).

58. Stott, V., "Collected Researches," Vol. XXIV, Standards of the National Physical Laboratory, London.

59. Stull, D. R. and Sinke, G. C., "Thermodynamic Properties of the Elements," American Chemical Society Advances in Chemistry Series No. 18, Washington (1956).

60. Volmer, M., Z. Physik. Chem., Bodenstein Festband, 863 (1931).

61. von Wartenberg, H., Berichte 39, 380 (1906).

62. Winterbottom. W. L. and Hirth, J. P., _J_. _Chem_. _Phys_. _37_, 784 (1962).

63. Walker, R. F., in "Vacuum Microbalance Techniques," _Vol_. _1_ (M. J. Katz, ed.) Plenum Press, New York (1961).

64. See any standard physical chemistry text.

APPENDIX A

CALCULATION OF THE MASS EFFUSING DURING COOLING

The Knudsen equation can be written

$$P_K = \frac{dm}{dt} \frac{(2\pi RT/M^*)^{\frac{1}{2}}}{aW} \, . \qquad\qquad A-1$$

The integrated form of the Clausius-Clapeyron equation[63] is

$$P_K = e^{A/T} e^B = f(T), \qquad\qquad A-2$$

where $\qquad\qquad A = -\Delta H_{vap}/T$

$\qquad\qquad B$ = integration constant.

A function $g(t)$ is defined which gives the instantaneous temperature of the cooling Miker cell:

$$T = g(t) \qquad\qquad A-3$$

But since we have $\qquad\qquad P_K = f(T)$

it follows that $\qquad\qquad P_K = f[g(t)] = h(t). \qquad\qquad A-4$

The Knudsen equation (A-1) then becomes

$$h(t) = \frac{dm}{dt}(2\pi RT/M^*)^{\frac{1}{2}} g(t)^{\frac{1}{2}}, \qquad\qquad A-5$$

or

$$dm = Wa(M^*/2\pi RT)^{\frac{1}{2}} \frac{h(t)dt}{\sqrt{g(t)}} \qquad\qquad A-6$$

Integration over the time of the cooling process yields the mass m_c effusing during this time:

$$\int_{m \text{ at } t_o}^{m \text{ at } t} dm = m_c = Wa(M^*/2\pi R)^{\frac{1}{2}} \int_{t_o}^{t} h(t)dt/g(t)^{\frac{1}{2}} \qquad\qquad A-7$$

Evaluation of the above integral requires a knowledge of cooling behavior of the cell, or $g(t)$. Experimental rate of cooling data were

obtained for several cells. Two observers were required for the determinations. The Miker cell was first heated to about 1500°C. One observer then cut the heating power (T_0, t_0) and recorded time intervals for the second observer who followed the cooling by means of optical pyrometer sightings into the cell orifice and signalled to indicate the instant a satisfactory reading had been obtained. This procedure was repeated until a sufficient number of readings was obtained. Cooling data appear in Figure 25 as a ln T-vs.-t plot. From the apparent fit, we obtain the function $g(t)$,

$$g(t) = T = e^{-kt}, \qquad\qquad \text{A-8}$$

where   k = slope of ln T vs. t plot.

Substitution of (A-8) into (A-5) yields

$$h(t) = e^{B}e^{(A/T_0)e^{kt}}, \qquad\qquad \text{A-9}$$

and expression (A-7) becomes

$$m_c = Wa(M^*/2\pi R)^{\frac{1}{2}} \int_{t_0}^{t} e^{B}e^{(A/T_0)e^{kt}}e^{kt/2}dt. \qquad\qquad \text{A-10}$$

With the substitution of variables $e^{kt/2} = x$, equation (A-10) becomes

$$m_c = [Wa(M^*/2\pi RT_0)^{\frac{1}{2}}/k] \int_{1}^{\infty} e^{(A/T_0)x^2}dx. \qquad\qquad \text{A-11}$$

With the further substitution of variables $Ax^2/T_0 = -v^2/a$, expression (A-11) becomes

$$m_c = [Wae^{B}(M^*/-\pi RA)^{\frac{1}{2}}/k] \int_{v_0}^{\infty} e^{-v^2/2}dv, \qquad\qquad \text{A-12}$$

where $v_0 = (-2A/T_0)^{\frac{1}{2}}$.

Equation (A-12) may be written for convenience as

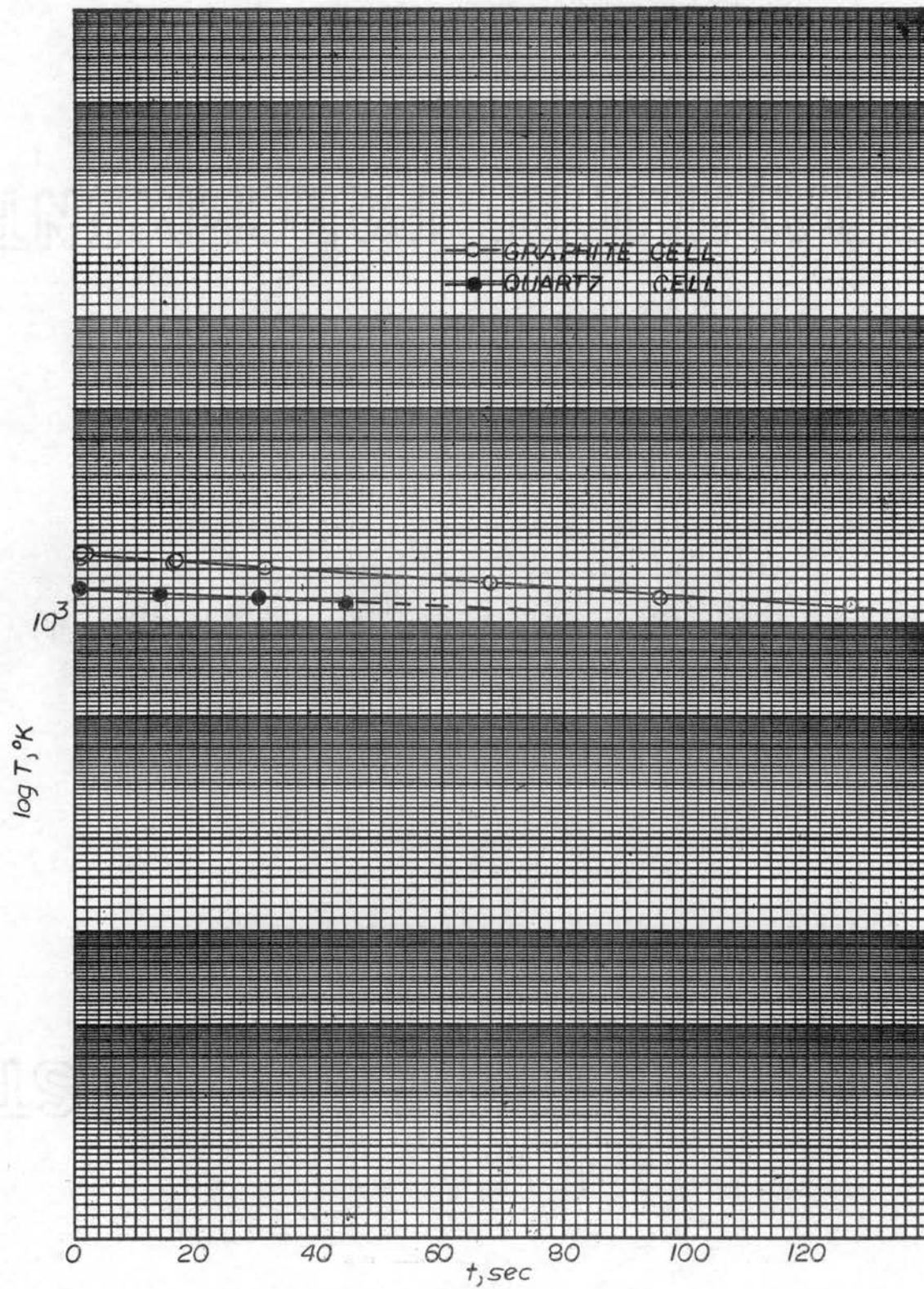$$m_c = K(M^*)^{\frac{1}{2}}I(v_0), \qquad\qquad \text{A-13}$$

Figure 25. Experimental Cooling Curve for Miker Cells.

where
$$K = Wae^{B}(1/-2RA)^{\frac{1}{2}}/k,$$
A-14

and
$$I(v_o) = 2(2\pi)^{-\frac{1}{2}} \int_{v_o}^{\infty} e^{-v^2/2} dv.$$
A-15

Substitution of (A-13) into (28) yields

$$P_R = 2g[m + K(M^*)^{\frac{1}{2}}I(v_o)]/af .$$
A-16

Substitution of equation (24) into (A-16) yields

$$P_K M_K^{\frac{1}{2}} = (M^*)^{\frac{1}{2}} 2g[m + K(M^*)^{\frac{1}{2}}I(v_o)]af$$
A-17

Rearrangement of (A-17) yields a quadratic with respect to $\underline{M}^{*\frac{1}{2}}$:

$$M^* + mM^{*\frac{1}{2}}/KI(v_o) - P_K af M_K^{\frac{1}{2}}/2gKI(v_o) = 0.$$
A-18

The vapor pressure and recoil force data for each run, i.e., each $\underline{T}_o$, must be substituted into equation (A-18) in order to obtain the corrected average molecular weight $\underline{M}^*$. Details of such a calculation follow for Run No. 42 for CaF_2.

The integral

$$I(v_o) = 2(2\pi)^{-\frac{1}{2}} \int_{v_o}^{\infty} e^{-v^2/2} dv$$

is in form identical to the so called normal probability function, which has been evaluated to six significant figures over a range of $\underline{v}_o$ values (National Bureau of Standards Applied Mathematics Series - 23). Thus a knowledge of $\underline{v}_o$ immediately yields the value of $I(v_o)$.

The value of $\underline{K}$ is a constant for a given cell and sample substance. For calcium fluoride the following data apply:

$W = 0.996$

$a = 0.02075$ cm^2

$k = 1.52 \times 10^{-3}$ sec^{-1} (slope of cooling curve)

$$\ln P = 18.33 - 46550/T$$

$$e^B = 90.0 \times 10^{12} \text{ (B in dynes/cm}^2)$$

$$A = -46550 \text{ deg}$$

$$g = 980 \text{ dynes}$$

$$f = 1.00$$

Substitution into equation (A-18) yields

$$M^{*\frac{1}{2}} = 1.05 \times 10^{-4} P_K/m - 4.38 \times 10^8 I(v_o) M^*/m \qquad \text{A-19}$$

For CaF_2 No. 42:

$$T_o = 1619^\circ K$$

$$P_K = 19 \text{ dynes/cm}^2$$

$$v_o = 7.60$$

$$I(v_o) = 2.96 \times 10^{-14}$$

Substitution into (A-19) yields

$$M^* = 76$$

Similar calculations, using (A-19), were performed for the other CaF_2 data to yield the $\underline{M}^*$ values in Table VI.

For the silver and tin data, the procedure is entirely the same, the only differences being those of constants $\underline{A}$, $\underline{B}$, $\underline{k}$, etc.

For the silver measurements with the graphite cell,

$$M^* = 7.54 \times 10^{-5} P_K/m - 4.62 \times 10^6 I(v_o) M^*/m; \qquad \text{A-20}$$

for the silver measurements in the quartz cell,

$$M^{*\frac{1}{2}} = 1.63 \times 10^{-4} P_K/m - 2.94 \times 10^6 I(v_o) M^*/m; \qquad \text{A-21}$$

for the tin measurements,

$$M^{*\frac{1}{2}} = 1.91 \times 10^{-4} P_K/m - 2.86 \times 10^6 I(v_o) M^*/m. \qquad \text{A-22}$$

There is good reason to think that a more accurate cooling law

will be available in the near future. Not only will the accuracy be improved, but it appears that the expressions for $\underline{M}^*$ will be simplified appreciably. This problem is under investigation in this laboratory at the present time.

VITA

James Edward Bennett

Candidate for the Degree of

Doctor of Philosophy

Thesis: THE MIKER TECHNIQUE

Major Field: Chemistry

Biographical:

    Personal Data: Born at Wink, Texas, November 27, 1935, the son of
        James G. and L. Leona Bennett.

    Education: Graduated from Lamesa High School, Lamesa, Texas, in
        1953; received the Bachelor of Science degree from Northwestern
        State College, Alva, Oklahoma, with a major in chemistry, in
        May, 1957; received the Master of Science degree from Oklahoma
        State University, Stillwater, Oklahoma, with a major in
        chemistry, in May, 1962.

    Professional experience: Graduate Teaching Assistant, Oklahoma
        State University, 1957-58, 1961; Graduate Research Assistant,
        Oklahoma State University, 1958-61, 1962-64; Assistant Professor
        of Chemistry, Arkansas State College, 1964-.